Abstract

This work aimed at constructing a powerful yet inexpensive instrument and use it to provide a new technique in the detection of the malaria parasite. A multispectral microscope using multiple light-emitting diodes as illumination sources was constructed. The issue of chromatic aberration in conventional microscopy was accounted for through special reflective optics. A broad spectral bandwidth ranging from 375 nm – 940 nm could therefore be used to provide illumination in three different geometries. The applicability of this instrument was tested as the malaria parasite was observed inside single red blood cells measuring transmittance, reflectance and scattering of light from the cell. True color representations of single blood cells were observed in which a clear distinction between an infected and healthy red blood cell was seen. Spectra from all geometries were extracted in which contrast was seen in each. A preliminary contrast function was also created to graphically represent the acceptance criteria for malaria in a 3-dimensional space. The results obtained not only provided good contrast for malaria, but also reliability in the instrument.

Besides the technical construction of the microscope as well as scientific investigation of the malaria parasite, a strong collaboration between several Third-World countries was formed to explore the emerging field of multispectral microscopy. The need for this type of instrument and research in these regions of the world cannot be disputed.

Table of Contents:

Introduction

One of nature's longest realized phenomena, yet only recently scientifically more completely understood, is light and the exceptional properties it carries. In the 20th century scientists such as Maxwell, Planck, Einstein and many more, not only managed to describe the behavior of light but also to figure out ways to control it. A burst of technological discoveries followed, rendering a path where lasers and light-emitting diodes (LEDs) emerged and incorporated well into research and commerce. Today we would undoubtedly be crippled if these techniques and tools were removed since they are well integrated in medicine, general communication, and infrastructure. The expectations of the future are even brighter where literally more efficient products are expected to emerge at an exponential rate. According to Haitz's law [1], the LED technology is expected to double every 18 months providing highly efficient lighting and saving tremendous amounts of energy. LEDs are also produced at a cost which nearly seems insulting compared to how they perform making it highly competitive them the market.

The prospect of a bright future is very appealing; however, it is of great importance that research can maintain a productive edge rather than being destructive to mankind. Unfortunately, much misplaced focus as well as anger has led us in many wrong directions, but most still have good intentions. The research and technology described in this paper is intended to serve as an aid for anyone who so desires to use them for good purposes, and to describe an instrument which could potentially be used for answering pressing questions within medicine, agriculture, and more.

Motivation

This Diploma Thesis describes a multispectral microscope based on LEDs. The motivation comes from the ability to utilize thirteen different illumination bands in combination with advanced detection. From this, a multispectral image can be obtained combining both spatial and spectral information. This is a recent combination of two independently evolving fields of study, spectroscopy and imaging [2]. The power of this technique is truly revealed when multi-variate analysis is performed using the processing-power of a computer and information can be extracted which was not originally seen. In comparison to the detectors used today, the human eye performs quite poorly. It is hard to imagine that we are surrounded by information we cannot perceive; however, it is an undoubted truth that it exists. In many cases, if this information had been known to us it could have been the difference between life and death. The LED microscope essentially acts to extend the sensitivity of the human eye beyond the optical region of the electromagnetic spectrum and create microscopic images potentially revealing desired information. Allowing us to probe into the ultraviolet (UV) and infrared (IR) regions enables us to observe vegetation, where for example chlorophyll reacts heavily to UV-radiation, and where medical applications find much interest in the region 550 nm – 900 nm [3]. This type of flexible research necessitates an instrument of this kind.

Microscopy has also developed significantly in the last one hundred years which will be discussed briefly at a later point. To properly use the instrument and acquire good results, relevant information about microscopy will be presented.

There is great motivation for conducting this type of research in the Third World where an instrument of this kind could potentially find answers to pressing questions within medicine where many lives could be saved. According to the Center for Disease Control and Prevention (CDC) in an April 2007 release, 41% of the world population live in areas where malaria is easily transmitted (particularly West Africa, Asia, Middle East, Central and South America, Oceania). CDC also states that each year there are 350-500 million occurring cases of malaria, out of which over 2 million die. The majority of the fatalities are children from Sub-Saharan Africa. Every 2 minutes the parasite claims a life (info from the CDC website).

Project Overview

This project entailed constructing an LED multispectral microscope derived from a previous prototype designed and constructed by Mikkel Brydegaard [4]. The main features added to the previous version are two more angular geometries of illumination as well as reflective, rather than dispersive, optics to minimize chromatic aberration.

During the construction period of the microscope, time was allocated to mechanical, electrical, and optical design. In addition to this, a 2-week workshop, sponsored by the International Science Programme (ISP), was held at the University of Cape Coast (Cape Coast, Ghana), where scientists from six Third-World countries (Ghana, Cote D'Ivoire, Mali, Senegal, Kenya, and Sri Lanka) participated to construct a microscope by themselves, for themselves. Part of the time there was also spent holding lectures and labs on how to properly use the microscope and make calibrated measurements.

After the workshop, three weeks were spent at Felix-Houphouet Boigny Polytechnique Institute (Yamoussoukro, Cote D'Ivoire) where studies were made on *plasmodium falciparum* (a form of malaria) using the microscope. This was done in collaboration with Prof. Jeremie T. Zoueu and his group.

This paper is organized in such a way that it gives all the information needed to construct and maintain an LED multispectral microscope, as well as providing brief physics relevant to understanding the instrument. It will also present the procedures and results from the research carried out in Cote D'Ivoire on the *plasmodium falciparum* parasite.

Collaboration

The project ran under the supervision of Prof. Sune Svanberg and MSc of El.Eng. Mikkel Brydegaard. A strong collaboration with Jeremie T. Zoeue (Professor at the Felix-Houphouet Boigny National Institute Politechnique, Yamoussoukro, CI), Hiran Jayaweera (MSc., University of Colmbo, Sri Lanka) and Benjamin Anderson (MSc., University of Cape Coast, Ghana), was very helpful.

Theory

The behavior of light is very intricate and is based on what might seem as rather controversial science. Its elusive behavior makes it hard to make complete measurements and to fully characterize how it interacts with a specific sample. General physics in areas of ray optics, wave optics, electromagnetic and polarization optics will be presented, and explained in enough detail for the purposes entailed by this project. Spectroscopy, and the techniques thereof, will also be discussed as they are important to understand for diagnostic purposes. Multispectral Imaging is a more specific aspect of image processing and will be presented with a little more detail. All the formulas are intended to either support theory or to give a clear mathematical picture of an example. Programming code as well as detailed electronics will be found in Appendix I.

1 Relevant Optics Theory

Ray optics explains how the optical components propagate light through the microscope in a very simplified model. It can help to draw general conclusions regarding magnification and geometric distances to focus, which helps much in the initial design of optical systems. The most fundamental equation is the lens formula (Eq. 1-1), which describes roughly how light converges or diverges through a thin lens. As an object is placed on one end of the lens, predictions of its magnification (Eq. 1-2) and whether the resulting image is real or virtual can be drawn. Unfortunately, light cannot be fully described by drawing straight lines, but it can give quite a good understanding of how it behaves. Another fundamental relation is Snell's Law (Eq. 1-3) and it describes how light behaves as it passes from one medium to another [5].

$$\frac{1}{f} = \frac{1}{a} + \frac{1}{b} \qquad \text{(Eq. 1-1)}$$

$$M = -\frac{b}{a} \qquad \text{(Eq. 1-2)}$$

$$n_1 \sin(\Theta_1) = n_2 \sin(\Theta_2) \qquad \text{(Eq. 1-3)}$$

n_1 and n_2 represent the refractive indices of the 1st and 2nd medium through which the light passes. Θ_1 and Θ_2 are the angles the ray makes to the normal

1.1 Polarization and its Effect on Measurements

In the middle of the 19th century, James Clerk Maxwell discovered that light is energy and comes from both an electric and magnetic field acting together. The electric field cannot exist without the magnetic field and vice versa. The two fields oscillate in exact phase perpendicular to each other and both orthogonally to the

direction of propagation. The electric-field component is what causes electrically charged particles in a medium to oscillate so it is of interest to characterize its behaviour. At any point, if a plane perpendicularly intersecting the wave in the direction of propagation, the resulting image would be two vectors, 90° apart with time-dependent magnitudes **E** and **B**. If the plane would be fixed in space (at the boundary between two media for example) and several wavelengths would pass through it, the electric-field vector would oscillate back and forth in its orientation and the light is said to be linearly polarized. If an additional wave is considered having a phase delay and/or a slight rotation around the axis in the direction of propagation, the light can be either elliptically or circularly polarized while either rotating left- or right-handedly. The polarization of light is a measure of the electric-field behaviour of a medium, and as the wave passes from one medium to another, the amount of energy passed will depend on the nature and orientation of the polarization [6]. This becomes important to consider when making microscopic measurements since frequently, glass slides are used to contain the sample from which light will be significantly reflected depending on the angle of incidence. The transmitted part of the wave will transfer the energy into the medium. The power reflectance (r) and transmittance (t) can be summarized in Fresnel's equations (which are derived from Maxwell's equations),

Fresnel's Equations

$$r_x = \frac{n_1 \cos\theta_1 - n_2 \cos\theta_2}{n_1 \cos\theta_1 + n_2 \cos\theta_2} \qquad \text{(Eq. 1.1-1)}$$

$$r_y = \frac{n_1 \sec\theta_1 - n_2 \sec\theta_2}{n_1 \sec\theta_1 + n_2 \sec\theta_2} \qquad \text{(Eq. 1.1-2)}$$

$$t_x = 1 + r_x \qquad \text{(Eq. 1.1-3)}$$

$$t_y = (1 + r_y)\frac{\cos\theta_1}{\cos\theta_2} \qquad \text{(Eq. 1.2-4)}$$

The subscripts indicate the projection of the power reflected (r) or transmitted (t) onto the x- and y-axis assuming the direction of propagation runs with the z-axis.

1.2 Dispersion

Electromagnetic radiation consists of a number of waves of varying frequencies added together creating wave-packets. The speed at which the envelope of the wave-packet moves through a medium is generally referred to as the group velocity (υ_g). The phase velocity (υ_p) is not quite the same thing and refers to the speed at which any point of any wave of the wave-packet propagates through a medium. The energy carried by the wave is used to oscillate the electrons in the medium at the same frequency as the oscillating envelope, which means energy propagates with the group velocity. The phase velocity is defined as the ratio of the

angular frequency, ω (which is related to the wavelength, λ, through ω=2πc/ λ) to the wave number, k (Eq. 1.2-1). The group velocity is defined as the ratio of rate of change of the angular frequency with respect to the wave number (Eq. 1.2-2) [5].

$$v_p = \frac{\omega}{k} = \lambda f \qquad \text{(Eq. 1.2-1)}$$

$$v_g = \frac{\partial \omega}{\partial k} \qquad \text{(Eq. 1.2-2)}$$

Where *f* is the frequency of the wave packet in the medium

From these equations it can be understood that the two velocities can either be the same or different since ∂ω does not have to be directly proportional to ∂k. This is determined from the wavelength-dependant dielectric properties of the medium. The implication of the above discussion is that different energies (wavelengths) will move through a medium at different velocities. This is an important phenomenon in optics and is called dispersion.

Light moving through optical components will disperse at various rates related by a quantity called the *refractive index* (RI). This property of a medium defines the optical density for a specific wavelength. Air is assumed to have a RI=1, whereas glass has RI≈1.5 (which makes sense since looking through a glass makes an image blurry because the light is more dispersed). Chromatic aberration causes problems when measuring with optical instruments since red light will pass through the optics faster than blue light. This is what lays the foundation for Snell's Law (Eq. 1 -3). Chromatic aberration will be discussed further in a later section.

1.3 Kramers-Kronig Dispersion Relation

The Kramers-Kronig relation can be applied to many situations in physics as it describes the cause and effect relation. It essentially claims that without cause, there cannot be a related effect. Of interest in optics is the Kramers-Kronig dispersion relation. The refractive index, *n(ω)*, can be described as a complex function having a real part, $n_{Re}(w)$ (depending on the phase velocity), and an imaginary part, $n_{Im}(w)$ (depending on a number of optical properties of the medium, including the absorption coefficient), according to Eq. 1.3-1 [7],

$$n(\omega) = n_{Re}(\omega) + i\, n_{Im}(\omega) \qquad \text{(Eq. 1.3-1)}$$

The Kramers-Kronig relation applied to Eq. 1.3-1 becomes

$$n_{Re}(\omega) = \frac{2}{\pi} P \int_{-\infty}^{\infty} \frac{n_{Im}(\omega')}{\omega' - \omega} d\omega' \qquad \text{(Eq. 1.3-2)}$$

$$n_{Im}(\omega) = -\frac{2\omega}{\pi} P \int_{-\infty}^{\infty} \frac{n_{Re}(\omega')}{\omega' - \omega} d\omega' \qquad \text{(Eq. 1.3-3)}$$

Where P is the Cauchy Principal value used for improper integrals so that they can be defined

As can be seen from Eq. 1.3-2 and 1.3-3, there is a dependency between the real and imaginary part of Kramers-Kronig dispersion relation. This means that one can be represented as an integral of the other and thereby only information regarding one can yield information about the other; in other words, a material whose refractive index is wavelength dependent must exhibit absorption [5]. The refractive index is the response caused by absorption. Hence, reflection data can reveal optical parameters of a material from the fact that part of the wave has been transmitted into the material as discussed in section 1.1. It is, however, necessary that the incidence is normal and that the sample is semi-infinite [7, 8].

In material science applications, measurements are generally made in transmission as well as reflection to gather data on the dielectric properties. However, when a sample is non-transparent or it exhibits Fabry-Perot interferences, it complicates things. In the former it is clear that only reflection measurements can be made, but in the latter, multiple solutions to the dielectric function can be obtained. In these situations, the Kramers-Kronig dispersion relation could be utilized to extract information [8].

These techniques were not applied in the main work presented here since the sample could be observed over the desired spectral range in both transmission and reflection. However, due to the flexibility of the microscope to several application fields, it is worth to consider these techniques if necessary.

1.4 Scattering

One of the most fundamental interactions of EM radiation with particles is scattering which gives rise to many optical phenomena. This is the reason why the sky is blue during the day and red at sunset; the reason why clouds appear white, and essentially the main reason we can see things [7]. As EM radiation interacts with a particle, not only can it re-emit the radiation but it can also scatter it in all possible directions. The specific behaviour depends on the type of particle and its size in relation to the incoming radiation. Rayleigh and Mie scattering are two types of elastic scattering giving rise to phenomena such as different colors of the sky, and the rainbow. Raman scattering (inelastic) is heavily used for diagnostic purposes in combustion physics to non-intrusively determine temperature, molecular concentrations etc. In this work, elastic scattering will be discussed as it becomes of interest to know how photons scatter in red blood cells. Mie scattering will be covered in brief detail since it is the primary approximation used when investigating red blood cells.

A single scattering event between radiation and a particle is considered to be random because of the wave-particle duality posed in quantum mechanics. An exact location of where the scattered photon will be cannot be determined, rather, a probability distribution must be used. In the event of several single scattering events, called multiple scattering, the behaviour can be better determined because an average can be calculated from all the individual probabilities. In the visible region, the wavelength of the radiation is very small in comparison to the macroscopic objects around us, which means photons will undergo multiple scattering. If the

particles of an object are packed densely together, photons travelling through it will undergo 'impacts' more frequently than they would moving through an object with lower particle density. In other words, the distance a photon travels between impacts will vary depending on how optically dense the object is (optically dense meaning that the separation of molecules of a medium is much smaller than the wavelengths in the visible region) [7]. The distance between scattering events is called 'mean free path' and is inversely proportional to the scattering coefficient. A highly diffuse object has a short mean free path, which means it has a high scattering coefficient and will appear foggy to the human eye. A perfectly diffuse object will scatter light evenly in all direction giving rise to what is known as a Lambertian distribution of light.

1.4.1 Mie Scattering Theory

Mie scattering theory describes the scattering event from any size spherical and homogeneous particle and is valid for all wavelengths and size spheres. However, it will not always be the best approximation as Rayleigh scattering provides a more accurate approximation when the particle diameter << radiation wavelength. Mie scattering theory is widely used in meteorology since the radiation wavelength from the sun is of comparable size to various particles in the atmosphere such as dust, water vapour, smoke, pollen and more. Due to Mie scattering, these particles reduce the visibility which would otherwise have been several 100km [9]. However, much interest is devoted to Mie scattering theory since it also seems to be the most common approximation for modelling light interactions with red blood cells [11-13]. Red blood cells are not spherical, but their homogenous disc-shape can be well approximated with Mie scattering.

1.4.2 Specular vs. Diffuse Reflection

As previously mentioned, light can be scattered in all directions, but what is then reflection? First, a distinction must be made between specular and diffuse reflection. After that the definitions can be fudged a little bit. The most common perception people have of reflection is what is classified as specular reflection. The word *speculum* comes from Latin and means 'a mirror or polished metal plate' [www.thefreedictionary.com]. A very polished surface (polished to the point where the size of the irregularities is smaller than the incoming wavelength) will 'scatter' the light in a highly predictable direction according to the law of reflection ($\theta_i=\theta_r$) [7]. This is specular reflection. As the irregularities of the surface increase in size in relation to the radiation wavelength, the reflected radiation will act more and more random. This random reflection is called diffuse reflection. An example would be observing an object reflected from the surface of a calm lake. The object appears well defined and clear as long as the water surface is smooth and clear. As soon as wind starts rippling the surface and progressively creating larger and larger waves, the reflection of the object disappears since the light from the object is now reflected in many different directions.

During measurements it becomes important to take these two types of reflection into consideration when using optical references. Since there is a frequent use of glass in microscopy (where the sample is contained), it is important to consider the effects of diffuse and specular reflectance and how these can 'intermingle'. See Fig. 1.4.2-1.

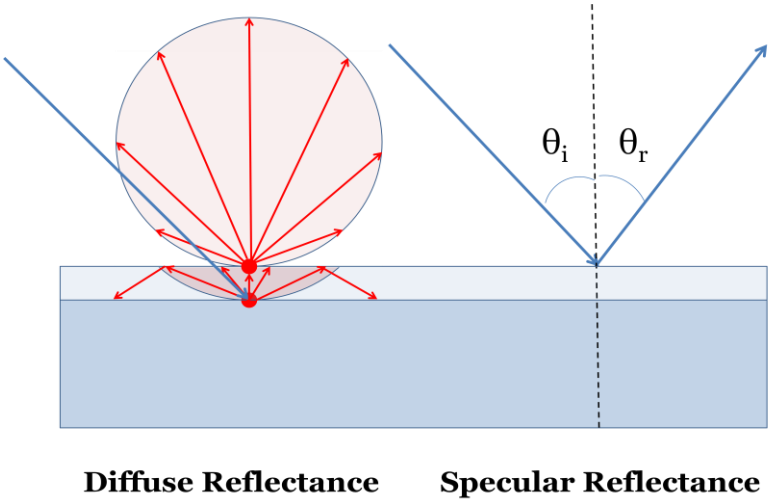

Fig. 1.4.2-1 A schematic showing a simplified sketch of the Opal Diffuser providing both diffuse as well as specular reflectance. Since it is impossible to draw all the points from which light emerges, only one point at each surface from which light spreads at a surface is drawn

1.5 Absorption: Beer-Lambert's Law

The Beer-Lambert Law is important to understand when making any kind of spectroscopic investigation since it comprises a fundamental part of the events occurring when light interacts with matter. As discussed previously, a photon can scatter off a particle in essentially any angle in relation to the incoming angle. If the energy of the photon matches any quanta allowed by the electronic configuration of the particle, the photon will be absorbed causing the particle to attain an excited state. From this point a number of things can happen which will not be covered here.

There are a number of ways the physics of absorption can be communicated, but an easy and common way to explain it is to compare the incoming and outgoing beam intensities to and from a medium. The ratio $T = I/I_0$ is referred to as the transmittance of a sample. Using this together with the molar absorption coefficient and the molecular concentration lumped up in one constant, μ_λ, and the distance travelled through the medium, *l, the* total absorbance, A_λ, is found by Eq. 1.5-1.

$$A_\lambda = -log\,(T_\lambda) = \mu_\lambda l \qquad \text{(Eq. 1.5-1)}$$

The wavelength dependency comes from the fact that molecules absorb varying quanta of energy depending on their molecular configuration, which will be discussed in the 'Spectroscopy' section. From Eq. 1.5-1 it is evident that absorbance

increases with increased molecular concentration, higher absorption coefficient, or longer path through the medium [9].

1.6 Object-Image Distortions

When an object is imaged through any sort of instrument, the process is subject to a number of distorting events causing the resulting image to become blurry; especially if an instrument uses a wide range of wavelengths to illuminate the sample. For each instrument, depending on the nature of the distorting event, mathematical functions can sometimes be constructed in order to correct or communicate the error due to the instrument. In this section, some of the most important distorting phenomena arising from diffraction and dispersion will be discussed without involving any specific mathematical functions.

1.6.1 Point Spread Function

In any instrument dealing with EM radiation, optical transfer functions should be discussed. They essentially communicate how well the instrument can 'handle' a signal from object to image, or how well it responds to an impulse. The most common transfer function is the Point Spread Function (PSF) which communicates how much a signal spatially blurs through the instrument, or how well it maintains contrast. Contrast is the carrier of information and the PSF is a measure of how well the system can maintain this [14]. According to quantum physical theory, a pulse of light can never be perfectly defined, and even if it could, it is still subject to diffraction and dispersion. It is therefore impossible to achieve a perfect relation with a ratio of 1:1 between object and image.

Illumination of a sample through an imaging system can occur in several ways, but what they all have in common is that the light has to emerge from some point, whether it is from the depletion region inside a semiconductor or the filament inside a light-bulb. Usually, what follows is a number of optical components which will shape the beam profile before it reaches the sample, and eventually the detector. Suppose light emerges from an aperture of measurable size. According to Huygen's principle, light comes from a very large number of points and the diffraction through the aperture will not be so evident since the aperture is much larger than the wavelength of the light. Dispersive optics can only become perfect in the diffraction limit and this is only true when the component is free from impurities inside and on the surfaces. The PSF is unique to each component and creates a linear combination for the complete system [15]. If all components were as perfect as they could be, there would still be a smearing of the edges due to the diffraction limit of each component which cannot be experimentally accounted for; See Fig. 1.6.1-1.

Optical components are never going to be completely free from impurities, nor will their surface be completely smooth in relation to their wavelength. It is therefore important to handle them with utter care to avoid scratches and fingerprints which definitely add to the PSF of a component and thereby the PSF of the whole imaging system, which in turn increase the 'blurring' of all images taken thereon [15].

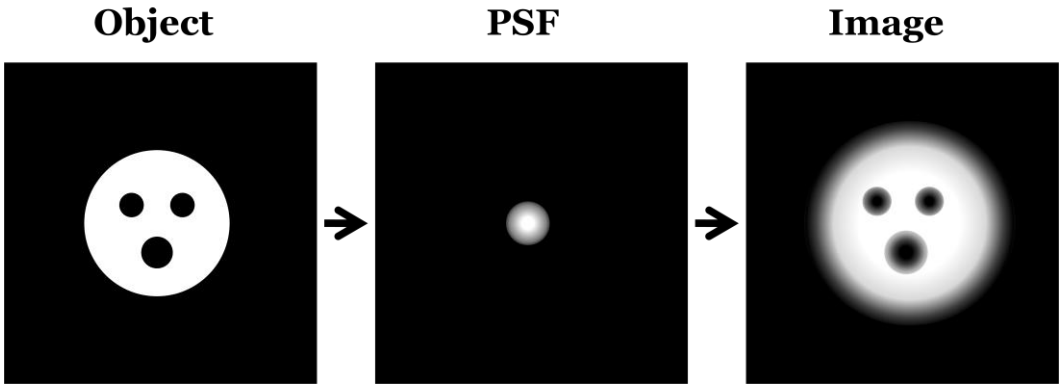

Fig. 1.6.1-1. Illustration of how a smooth PSF of an imaging system can alter the image. Of course, the PSF can be uneven which is often caused by rough irregularities in optical components such as a cracked lens

1.6.2 Chromatic Aberration

The phenomenon of chromatic aberration arises from dispersion which is not a property of the radiation but rather the medium. The dielectric properties of a medium are dependent of the energy; hence different wavelengths will experience different refractive indices as discussed before. This is a major problem in imaging systems using a broad range of spectral bands. It is clear that the more optical components a system has, the more prominent the chromatic aberration will be (unless achromats are employed). Also, if the media of the components have optical absorption properties such that it has a steep gradient over a short wavelength region the chromatic aberration will be more significant. Most optical materials are transparent in the visible region, but exhibit absorption when entering the UV region [5]. In order to have transmittance in this region fused silica or quartz is often used to create lenses. Absorption in the UV also causes the refractive index to increase, but only if the refractive index can be represented by the complex the function in Eq. 1.3-1. Therefore, to get less chromatic aberration a lens should be chosen which varies little in refractive index over the spectral region of interest in order to minimize the spectral blur. Fig. 1.6.2-1 shows a pedagogic example of how a lens disperses white light.

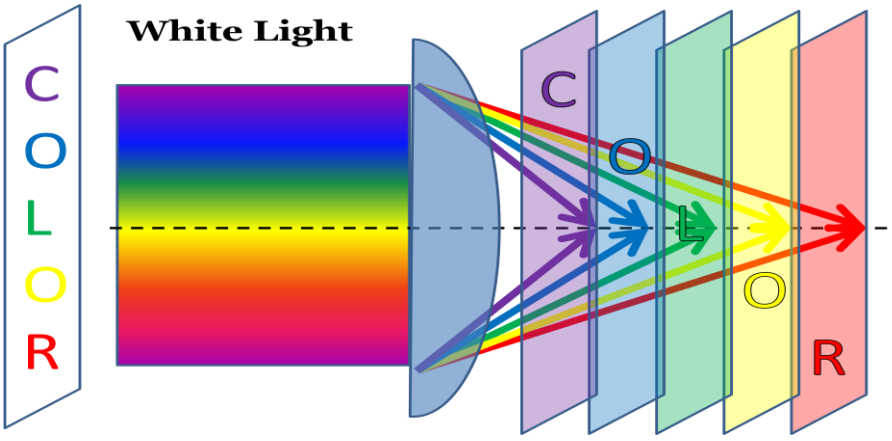

Fig. 1.6.2-1 A pedagogic example of how chromatic aberration works. Not all lines are included, only the ones which need to refract most in order to reach their intended focus.

2 Spectroscopy

Spectroscopy is the use of electromagnetic radiation to study the chemical composition of matter. An atom will absorb energy depending on its electronic configuration and can therefore be spectrally characterized. The laws of quantum mechanics govern which discrete energy configurations a specific atom or molecule can have and thereby determine which wavelengths it can interact with. Over the entire EM spectrum different types of interactions occur. At low energies observations are made of groups of oscillating charge carriers in solid matter. As energy increases, individual molecules start to rotate and eventually vibrate. The energy is on the order of 10^{-3} eV for rotations and 10^{-1} eV for vibrations which correspond to the microwave and mid-near IR regions, respectively (1 eV is the energy required to accelerate 1 electron of charge 1.60217646 x 10^{-19} C through a potential of 1 V). When the energy is increased another factor of ten, electronic transitions occur which can be detected by the human eye. This corresponds to the visible region and covers only a small fraction of the entire EM spectrum. At higher energies electrons start moving so violently that they manage to overcome the strong forces keeping them in orbit of the atomic nucleus and escape in a process known as ionization (the force is known as the 'electromagnetic force' and is not to be confused with the 'strong force' keeping nuclei together). So spectroscopy does not only involve detection of radiation but also charged particles. The photoelectric effect, Compton scattering, and pair production are examples of processes occurring at higher energies where particles are emitted. Using a database of information of how various atoms and molecules interact with energy of varying magnitude, spectroscopy becomes a powerful technique with nearly endless applications.

2.1 Illumination-Detection

Understanding how light-matter interactions work is only half of the task as one must also figure out a way to probe and detect desired information. A spectroscopic investigation can be divided into three parts: source illumination (E_λ), sample emission (R_λ), and detection (S_λ), according to Eq. 2.1-1 [4].

$$U_\lambda = \int_0^\infty E_\lambda \; R_\lambda \; S_\lambda \; d\lambda \qquad \text{(Eq. 2.1-1)}$$

The resulting signal (U_λ) is a linear combination of the three parts. In an experiment E_λ and S_λ can be controlled by the experimenter while R_λ is a property of the sample comparing the emitted intensity to the incident intensity. The information available from the sample is essentially infinitely resolved (only limited by fundamental forces of nature), so the question is how well it can be extracted with an illumination-detection system. If there is much information with regard to how a sample is illuminated, i.e. having many sharp spectral bands illuminating the sample in a controlled manner, there is little need having a detector which also can spectrally resolve the received information. This is also true in the opposite case. For example,

using a tunable laser together with a grating spectrometer is unnecessary where, in most cases, either the spectrometer could be replaced with a monochromatic detector (records intensity levels on a grey-scale), or the laser with a broad white light source. These considerations are important for reducing costs and making more efficient instruments. There is, however, one case where illumination and detection cannot be substituted for each other and that is when the sample emits significant fluorescence. A vegetation sample illuminated with 405 nm radiation will emit broad radiation at longer wavelengths closer to the IR-region. A monochromatic detector only measures intensity along a gray-scale and will therefore record a total intensity as a response to the elastic sample emission at 405 nm as well as the broad fluorescence signal generated by the fluorophores in the molecules. Similarly if a broad radiation source is used with a spectrometer, the emission spectrum will show an increased signal in the IR due to the fluorescence coming from the UV. To overcome this problem, and also to study the fluorescence behaviour, excitation-emission spectroscopy can be applied where both the illumination and detection is tunable and well resolved.

Since the EM spectrum covers such a vast range of energies, there is no single instrument which can either efficiently detect or act as a radiation source for the entire spectrum. In each region, a specialized instrument for either detection or illumination is required. There are a number of different illumination sources ranging greatly in cost and efficiency. Laser sources produce very narrow emission lines while an LED produces a significantly wider emission line but is sometimes adequate to perform the spectroscopic task at hand. There is a significant price difference between the two. The region of interest to this project is over the UV-Visible-NIR region where LEDs suffice to reveal relevant information in most solid-state materials.

2.2 Multispectral Imaging

With the understanding of how EM signals arise at a microscopic level and how this signal can be captured at a macroscopic level, the discussion can progress to deal with what is called multispectral imaging. We now understand that the amount of information available is nearly endless so it would be highly time-consuming and inefficient to try to collect data from the entire EM spectrum. An analyzing device is therefore made with a certain number of spectral bands in the regions of highest interest for the intended experiment. In conjunction, the imaging device is able to simultaneously collect spectral data from several spatially discretized regions, which leads to simultaneously collecting spectra at many points in a two-dimensional image. This creates a three dimensional array of data containing both spectral and spatial information [4, 16]. Once all the information is captured and stored, computer-processing techniques can arrange the data in ways such that the desired information can be extracted, yielding chemical and physical as well as spatial properties of a sample [17].

The purpose of creating a multispectral image might not be clear unless the reader understands some elements of vision. It is also necessary to disconnect

conventional thinking of what color is and how it is perceived. There are also some aspects to image processing needed to be explained in order to connect all the relevant facts.

2.3 Vision

Human vision is only sensitive in a small fraction of the electromagnetic spectrum. The human retina has three types of cones which are sensitive to red, green and blue. With these three spectral bands, humans can see 'colors' in the range 400 nm - 700 nm roughly. The eye is most sensitive around 580 nm (roughly the color yellow) which is the where the Planck radiation from the sun peaks. 470nm is generally accepted as 'blue' and 630 nm as 'red'. Within this range, the eye is very sensitive as there are distinct differences between blue, green, yellow, orange and red, which all lie in this 160 nm region. From 400-470 nm everything looks more or less blue and similarly from 625-700 nm where it all looks more or less red. The reason colors appear the way they do is because of the sensitivity of the eye. In fact, the colors could not even be communicated unless given names understood by all; instead of saying 470 nm, we say blue. Everything humans see is some sort of composition of the three spectral bands from the cones on the retina. If we had more spectral bands, the world would look completely different as more 'information' would be visible to us. For example, birds have 4 spectral bands and the mantis shrimp has 12 [17]. How these animals view the world cannot be communicated, but it can be understood as will be discussed in the Multivariate Analysis section.

With more spectral bands, more nuances can be communicated; essentially meaning the electromagnetic spectrum can be more resolved in a specific region. With access to either a broader or more resolved spectral range, more information can of course be extracted. On the retina there also exist rods which function to resolve varying intensities of light. As an example, suppose the rods could distinguish between 10 intensity levels in conjunction with the three different cones. This means that the eye could distinguish between 10^3 different hues of colors. If an additional spectral band was added, there would be a factor 10 more 'colors' or if the sensitivity of the rods was increased to distinguish between 100 intensity levels, there would be 1 million, which is in fact matches the sensitivity of the human eye [18]. The amount of information available therefore increases drastically with every added spectral band or if the intensity can be better resolved. Collected information can easily be so large that it gets hard to process.

In an instrument it is important to understand that the spectral bands need to be added efficiently meaning that they should not overlap too much where the same information ends up being detected twice. They should also not be placed too far apart since the resolving power is then lost.

2.4 Image Processing

A digital image generally consists of a spatially defined region filled with discrete, square elements called pixels. The image serves to present information

which should be well communicated to the viewer. Each pixel will take on a numerical value relative to the light intensity captured by the imaging system, e.g. the camera. Depending on how well the camera can resolve the light intensity, represented by the bit-depth, the values will range between $0\text{-}2^x$ where 'x' is the bit-depth. For example, a camera having 8-bit pixel-depth can discretize light intensity into 256 separate bins, whereas a 12-bit camera can discretize light intensity into 4096 bins. The intensity range is generally referred to as the *dynamic range*. Similar to the way more spectral bands increase the spectral resolution, a higher bit-depth increases the dynamic resolution. It becomes of interest to have a highly resolved dynamic range when using software tools to enhance image quality or remove unwanted features. Any intensity too high for the camera to register will automatically fall into the last bin, thereby representing a saturated value. It is important to take this into consideration when taking any scientific image. For example, in dark field microscopy (discussed in the 'Optical Microscopy' section) where the signal of interest will be brighter than the background, it becomes very important not to saturate the image as important information is then lost. In bright field microscopy the background is brighter than the sample and less important information is lost in the saturation. However, it should be of general practice never to saturate an image or do so to a minimal extent. Fig. 2.4-1 gives a good overview of the different discretizations a signal can be subject to [4].

Discretization

Subject to discretization:	Light intensity	Light energy	Space	Time
Domain:	Dynamical -	Spectral -	Spatial -	Temporal -
Discretized by:	Bits	Spectral bands	Pixels / Voxels	Frames
Resolution:	Dynamic -	Spectral -	Spatial -	Temporal -
Res. limited by:	Signal to noise ratio / photons	Channel / illumination bandwidth	Point spread function	Exposure time / flash envelope
Range:	Dynamic -	Spectral -	Field of view	Recording time

Fig. 2.4.1: The table above shows how a signal can be subject to different discretizations in different domains. [4]

2.5 Image Acquisition Procedure

The LED microscope is equipped with thirteen wavelength specific illumination sources working in combination with a monochromatic camera. In the image acquisition process a gray-scale image is saved for each spectral band. Using MatLab® each image can be viewed individually or combined with two other images creating either a true image or a false color image. A true image is one where the gray-scale images from the red, green, and blue spectral bands are combined in a

similar fashion as they are in our brain. The result is an image of how it would be perceived and understood by a human [18]. Any other combination of three images provides a false image. False images only provide an interactive way for viewing a sample differently and to make general sense of how a sample interacts with light in the UV and IR regions. The real power lies in what is called multivariate analysis discussed below. A more detailed procedure of the acquisition procedure is found in Appendix II.

2.6 Multivariate Analysis

In any sort of scientific experiment, data is collected and analysed to reach some conclusion. Generally, results generated from an experiment are individually analyzed. As computers emerged in the 70's, new mathematical methods developed which served to complement the physical analysis. A computer's ability to quickly and accurately compute heavy algorithms made it possible for multivariate techniques to work. Since then, these techniques have developed and serve as major complementary techniques.

Multivariate analysis (MVA) involves simultaneous inspection of several variables. Humans, to a limited extent, implement this type of analysis daily. 'Is it an orange or is it a tennis ball?' one might ask. Although the answer is quite trivial, the analytical process our brain undergoes can very well be called MVA. A number of experiments can be conducted to determine whether this round object is eatable or if it is meant for smashing down a court. The first investigation is generally made with our eyes, which most of the time is enough for us to decide. However, the possibility of course exists that someone could have painted either the tennis ball or the orange to appear as the other in a very convincing way. A second experiment would perhaps be to smell the object and see if it has scent of citrus or rubber. Again, this could have been manipulated to trick the experimenter. A number of tests can be performed and taking the 'results' from all and simultaneously analyzing the object it is obvious that the experimenter becomes more and more sure of what the object is as more variables are considered (through more experiments). Some experiments will give more contrast between the two potential answers than other experiments. The shape of the object might not reveal as much information as the spectral appearance. This is a very trivial and more pedagogic example; however, it explains how MVA works in general.

There are a number of multivariate techniques and one which will be discussed here is called Principle Component Analysis (PCA). This technique involves restructuring the dimensionality of a sample and creating a new, more natural coordinate system for the subject. Each variable is introduced orthogonally to the others in order to maintain individuality and reduce co-variance between the variables. If they are all orthogonal, one can accurately say that variance along a certain dimension pertains to a specific variable, and only this variable. A coordinate system with more than three orthogonal axes is quite impossible to visualize. However, mathematically it makes complete sense and essentially endless

dimensions (variables) can be implemented because the limitation lies in the amount of data collected. These orthogonal axes are called Principle Components (PC). As discussed in the above example, there is going to be different variances depending on the experiment performed which translates into PC's having different weights in the complete analysis. The first principle component (PC1) should carry most weight meaning its variance contributes the largest variance in the result sought. PC2 follows with the second most variance and so on. At some point adding another PC contributes very little to the final result and can be considered as noise [17].

2.7 Calibration and Optical References

When making any sort of measurement the results need to be properly communicated to the public. The human mind is constantly putting things in frames of references to make more sense of the things occurring around us. A chair placed on the floor is generally accepted to be without movement. That is only true in relation to the already moving Earth it rests upon. However, referring the movement of the chair to the sun, it is all of a sudden (along with everything else on Earth) moving at several km/s. Hence it is important not only to make a measurement, but to also communicate it properly in a frame of reference generally accepted.

In spectroscopy it is of interest to measure various light intensity levels from a sample. With any single measurement it is impossible to draw a conclusion regarding how much a sample absorbs, scatters, or reflects unless the measurement is carried out in an extremely controlled environment (which is only idealistic). A starting point is to determine the spatial range through which the instrument can even detect a signal. Most instruments can only cover a fraction of the full angular spread (unlike for example the integrating sphere). For example, a telescope probing deep into space can only cover a mere fraction of the stellar sky, and much information is missed. Once decided, the detection limits can be communicated and a spatial reference can be set.

Some consideration is required when setting the light intensity references. Depending on the type of experiment, it is not necessary that the signal is referred to a universally accepted value. Only when it is desired to make a universal statement such as 'Sample X reflects Y% of the light at wavelength Z' is it necessary. This can be a very tough statement to make as many factors must be accounted for. Making measurements on human red blood cells (RBCs) is a good example where simplifications can be made. Since the blood carries many of human diseases it becomes hard to universally define what healthy blood really is. All humans living under various environmental conditions develop natural resistances depending on the place they inhabit giving different 'normals' depending on geographical region. It is therefore tough making a universal claim of how light interacts with healthy RBC, not because of difficulties in conducting the experiment, but rather due to making a proper definition. However, in this case one could pose the question whether it is relevant to make a global claim at all. Is it detrimental to the final conclusion that the absorption spectrum of RBCs, for example, is determined in a universal frame of reference? Determining whether an RBC is infected by a parasite only requires a

separation between an infected and non-infected RBC within the same blood. Normalizing to the same blood sample thus cancels many factors which simplifies the definition.

When making various types of measurements on the same sample (the case when characterizing absorption, scattering, and reflection), there is motivation behind using the same reference for all measurements. If using different references for each measurement, of which each is not connected to any reality, the experimenter cannot draw any conclusion beyond that of what the references allows. The conclusion, 'A fern leaf reflects twice as much as an oak leaf' only relates the two leaves to each other. If this is the extent of what the experiment sought to prove, there is no reason to go any further. It is crucial to understand that this is quite limited information and the result cannot be related to anything beyond this specific experiment.

In conclusion, there needs to be a known frame of reference from which a conclusive measurement can be made and communicated to the public.

3 Optical Microscopy

Optical properties of glass were early studied by Arabian scientists who utilized them to direct and magnify light. Since, optical magnifying tools have developed quite impressively and in more contemporary times, various types of microscopes have been introduced in order to probe deeper and observe smaller components of everyday life. 150 years ago, optical microscopes were the only type and could resolve images on the μm scale. Today, that resolution has increased by a factor of 100 [10].

Over this vast time period most of the development has taken place within optical configuration or general techniques. Not only until the last couple of decades, with the invention of the laser and LEDs did the illumination side receive much priority. Tungsten bulbs providing broad, white illumination have essentially been used since the time of Thomas Edison; mercury and xenon arc lamps have been used for fluorescence microscopy since their introduction as well [19]. Another significant development for microscopy, and imaging in general, was the introduction of CCD (Charged-Coupled Device) and CMOS (Complementary Metal-Oxide-Semiconductor) imagers. These types of cameras today provide exceptional resolution of imaging in the spatial, dynamic and temporal domains. Assisted by the processing power and user-friendly interface of a personal computer, very helpful tools have been constructed. Combining the aforementioned techniques, much more information can be extracted from a sample. The spectral information has become equally, if not more, important than the spatial information, especially when combined and the spectral information comes from regions human eyes cannot perceive. In the presented work a very unique LED multispectral microscope has been constructed capable of extracting spectral information simultaneously from millions of spatially resolved pixels. This information can further be processed on a computer in order to reveal very interesting results.

This section will include a brief section of the different modes of operation. The difficulties faced during the design phase of the project will be covered in the discussion at the end.

3.1 Modes of operation

In most optical diagnostics, the aim lies in extracting all the information possible from a sample, which is generally impossible. In spectroscopy the aim is to account for all photons emitted and to be able to explain whether they were absorbed, scattered, or re-emitted as fluorescence. Although a tough task, providing the capability of measuring scattering and reflection in addition to transmission, advances the LED microscope significantly over a conventional transmission microscope. A photon can scatter from a sample in every direction. In the images below the backscattering in bright-field and darkfield is not drawn since there is no detection on this side. For reflection it is only the backscattering and specular reflectance that is measured. Also, due to the type of objective used, the different modes of operation differ slightly to conventional definitions. The figures represent the modes as they operate in our system.

3.1.1 Bright Field Microscopy

Although the first type of optically magnified observation occurred with reflected light using magnifying glasses with the sun illuminating a sample, the most common way has become to observe samples in transmission. Transmission microscopy compares the incident light from the source to the transmitted light from the sample according to Beer-Lambert's Law (Eq. 1.5-1). However, to reach a concrete conclusion, either l *or* μ_λ should be known. In this mode the light that is not absorbed by the sample and captured by the detector (eye, camera, PMT etc) will be brighter than the absorbed areas making the background bright. Fig. 3.1.1-1 shows the setup for detecting transmission.

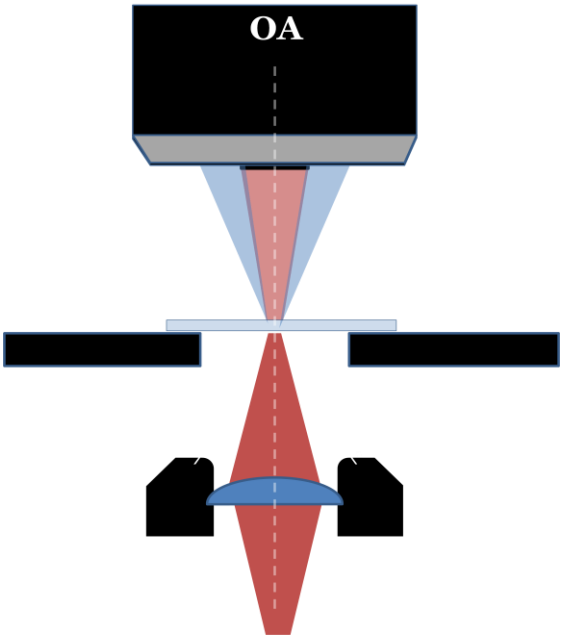

Fig. 3.1.1-1 Bright Field setup. The design shapes the beam so that it is detected although there is a region in the middle blocking the signal. Therefore, absorption can be measured to a satisfactory extent.

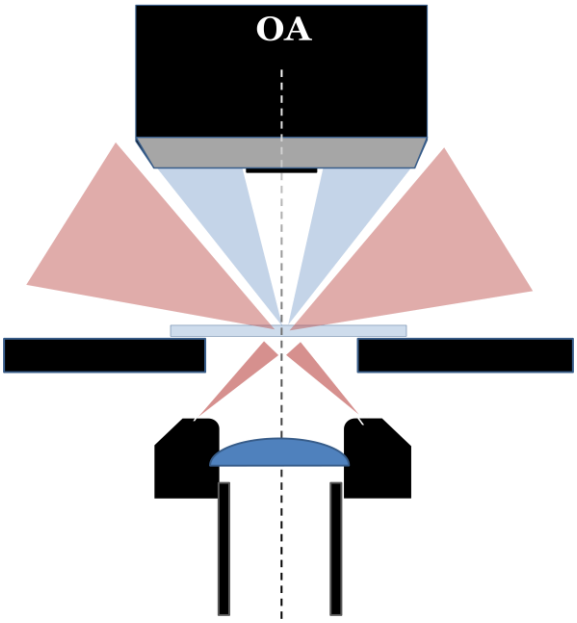

Fig. 3.1.2-1 Dark Field setup. The intention of the drawing is to show that without a sample, the incident light would miss the objective. Only light scattered into the objective is detected, but scattered photons may also not be detected as illustrated by the red regions.

3.1.2 Dark Field Microscopy

To make dark-field measurements in a microscope one needs to arrange the illumination source so that the transmitted light just passes the objective and no light is detected in the absence of a sample. Ideally, light should only be detected in the presence of a sample off which light is scattered into the objective (Fig. 3.1.2-1). This gives a decent measure of how a sample scatters, however, light is obviously scattered into many other directions where there is no detector so a full scattering profile cannot be made in this type of setup. The detection limit of the objective needs to be incorporated to communicate the angular region through which scattered photons are detected (will be discussed in the 'Sensitivity Lobes' section). In a dark field image the background will be dark and the detected scattering agents of the sample will be bright.

3.1.3 Reflection Microscopy

As the name implies, reflection microscopy measures the light that is reflected back in the same general direction as the incident light (within the numerical aperture of the objective). For this mode of operation a beam splitter is used since both the excitation and the sample emission partly travel the same way but opposite direction and need to be separated (Fig. 3.1.3-1). The type of objective used will be discussed in more detail at a later point, but it is worth mentioning now that due to its configuration it collects all specular reflectance from the object plane as well as any diffuse reflectance within the detection limits of the objective. Careful consideration is required when using glass slides and cover glasses since these provide strong specular reflectance and may cloud the signal from the sample of interest.

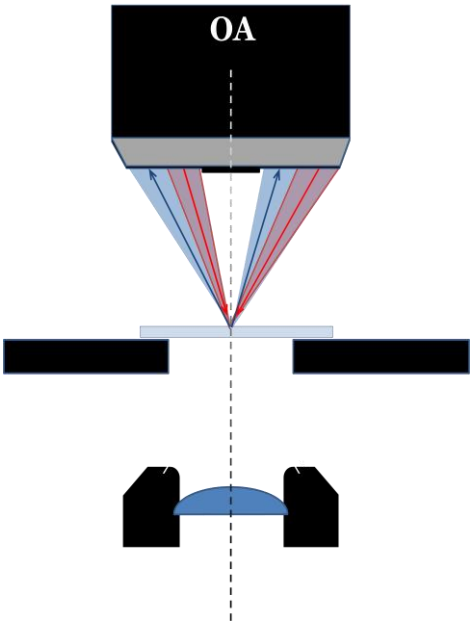

Fig. 3.1.3-1. Reflection setup. The signal is detected according to the law of specular reflection with a slight variance. The colors indicate that a photon can be detected incident from both sides of the objective.

3.1.4 Sensitivity Lobes

Discussed in a previous section, a photon can either scatter or be absorbed by a particle. Depending on the shape of the object, one might need to distinguish between forward scattering and backscattering. Objects such as RBCs have a disc-like shape and will therefore exhibit different behaviour between forward and backward scattering as discussed. It also becomes important to be able to identify through what spatial range the system can detect a signal. There is not a single instrument which can account for the entire angular distribution of possible scattering directions

The LED microscope is capable of illuminating a sample in three separate geometries so some boundaries should be considered between them. In the least, one detection region shouldn't be a linear combination of another. To start, the detection region of the objective should be calculated. Then the spatial emission distribution from the three modes should be calculated and a conclusion should be drawn where the boundaries should be set. Knowing the numerical aperture (NA) and working distance (WD) of the objective as well as some geometric distances, the sensitivity lobes of the system can be calculated for all three regions. A method for measuring the different sensitivity regions for each geometry will be explained in the 'Measurements & Results' section. The sensitivity regions can be communicated in a number of ways, one of which is plotting it in polar coordinates. For example, an angular geometry which is sensitive between ± 25°, will result in the polar plot in Fig. 3.1.4-1.

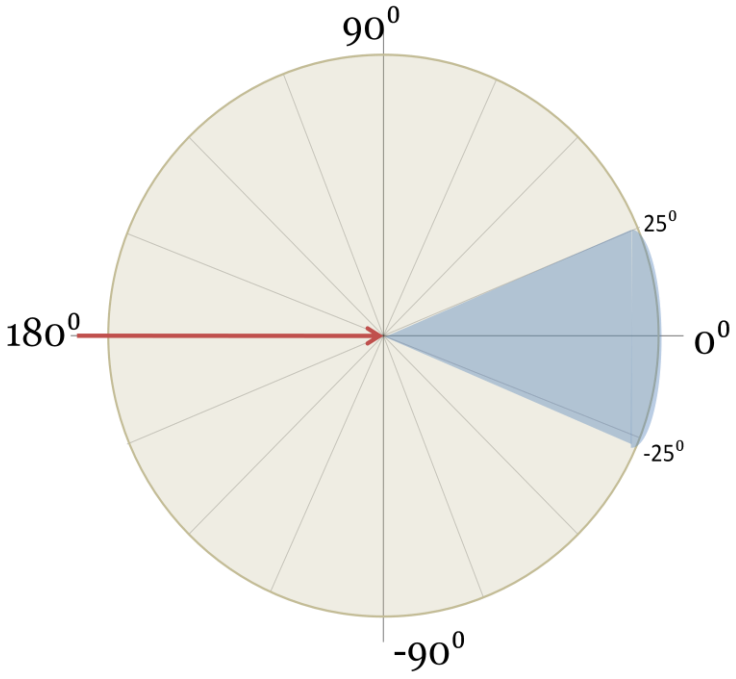

Fig. 3.1.4-1. The sensitivity 'lobe' defined above applies to photon scattered 25° from its initial trajectory in either direction.

3.2 Optical Properties of Red Blood Cells

Red blood cells (RBCs) are constantly moving throughout our body carrying oxygen between the lungs and our organs. They contain a chemical protein called hemoglobin, which not only carry oxygen to the organs, but also bring the remaining carbon dioxide to be exhausted. Hemoglobin is one of the strongest absorbers of light in our body and it exhibits significant dispersion throughout the visible region [11, 20]. The absorption spectrum of both oxygenated and deoxygenated hemoglobin shows a weaker absorption around 630 nm which is why our blood appears red [17]. Since RBCs and their movement around our body is an essential part to our well-being, any anomaly can cause drastic disorders to our health. The central aim of this project is to study the optical properties of an infected RBC without the use of chemical stains and primarily determine if a parasitic infection can be discovered spectrally. The use of stains have shown to cause problems when photobleaching (photochemical destruction of a fluorophore), interference with metabolic activities inside the cell, and non-uniform binding to molecules yield incorrect results [20].

This section will discuss the theoretical spatial shapes as well as optical properties of RBCs and which approximations could apply. A deeper look into the various scattering events will also be presented as well as a brief overview of the *plasmodium falciparum* parasite and its life cycle. Since hemoglobin is the main building block of the RBC giving rise to the optical properties, discussion of this protein will also be included.

3.2.1 RBC Shape and Analytical Implication

Before any extensive modelling is made of an RBC it is important to decide its physical shape and thereafter apply the proper scattering theory. It is known that RBCs are disc-like objects of diameter between 6-8 μm and thickness of 1.5-1.9 μm [Wikipedia: 'Red Blood Cell']. Unlike other biological cells having a nucleus and other organelles giving rise to complicated refractive-index distributions, RBCs have no internal structure which makes it easier to apply general theory of how light scatters [12, 13]. This fact also makes it easier to detect structured elements inside the RBC, such as a parasite. An RBC consists of a thin cell membrane with thickness 7 nm and a refractive index of 1.46. Inside the membrane is a homogenous aqueous solution of volume 70-100 μm^3 [21] consisting mainly of hemoglobin, salts, and other organic compounds.

The three fundamental factors to consider when analyzing a blood cell are the shape of the RBC, the angle of the incoming light, and the refractive index [13]. If one is satisfied with assuming a spherical shape, the angle of incidence plays a smaller role and Mie Scattering theory can be applied. Unfortunately, the shape of an RBC is more disc-like and thus creates a heavier dependency on the incoming angle. The Rayleigh-Gans scattering theory applies better to disc-shaped objects; however, one of the requirements is that the size of the object should be 20% or less of the wavelength used which is definitely not true in the case of RBCs being probed with light (400 nm – 700 nm). Although this requirement fails, one can still obtain

qualitative results which agree well with reality [11]. Further, there needs to be a distinction between forward scattering and backscattering of light as these behave quite differently. It has been theoretically shown that the forward scattering will depend mostly on the three-dimensional shape of the model as well as the thickness in the direction of the incoming light, also known as the optical thickness [12]. The backscattering will, on the other hand, depend heavily on the shape of the surface of the incident light, which can be understood from basic optical theory (Eq. 1.1-3). Oblique incidence will yield less backscattering than normal incidence. If an experiment seeks to measure mainly backscattered light, a spherical model is perhaps not ideally suitable. Therefore, under the assumption of a disc-shaped RBC, the forward scattered signal will vary with intensity whereas the backscattered signal will vary with angle of incidence.

Another important factor to consider is that RBCs act as single scatterers. The Henyey-Green function is often used in biological tissue modelling and is based on the assumption of multiple scattering. Applying the Henyey-Green function to modelling of an RBC will yield a weaker forward scattering and a larger side scattering, which is not suitable for single RBC analysis (these experiments assumed forward scattering within 15° to the normal) [12]. Analyzing single RBC requires that the distance from the center of the RBC to the surface of a neighbouring RBC is at least twice the size of the maximum diameter of the largest spheroid [12].

3.2.2 Optical properties of Hemoglobin

Hemoglobin is a protein strongly absorbing visible light. It is the major constituent of RBCs and the reason why blood appears red. Also very characteristic to blood, and hemoglobin in particular, is a strong absorption centered at 405 nm called the Soret Band [9]. This is a revealing characteristic of RBCs so it is worth keeping this in mind. As the shape of the RBC plays a crucial role in how the incoming light behaves when striking the surface, hemoglobin mainly gives rise to the refractive index of the cell. Due to the thin membrane and the aqueous hemoglobin solution inside, RBCs are quite deformable, which they need to be in order to smoothly flow through our body [13]. Morphological changes of the cell can inhibit the flexibility of the cell which can cause a stroke as there is a clog in the blood stream. As discussed above, since hemoglobin essentially determines the refractive index of the cell, varying concentrations will therefore yield variations in refractive index from cell to cell [13]. Depending on the instrument used, this could be an important factor since these variations in RI could mean that a signal is not detected within the acceptance angle of the objective used in the system [14].

Regarding absorption of hemoglobin to light, the Kramers-Kronig dispersion relation relates the imaginary part of the refractive index (n_{Im}) to the molar absorption coefficient (ε_μ) according to Eq. 3.2.2-1

$$n_{Im} = \ln(10)\frac{\lambda}{4\pi}\varepsilon_\mu c \qquad \text{(Eq. 3.2.2-1)}$$

The reflected signal depends on the refractive index according to Eq. 1.1-1 and 1.1-2, and can therefore be used with Eq. 3.2.2-1 to find the absorption spectrum of the sample. Since RBCs exhibit strong backscattering, its absorption spectrum can readily be obtained from only reflectance data.

3.2.3 Plasmodium Falciparum (malaria)

The *plasmodium* family is rather large with over 200 different species infecting both animals and humans. Out of the ten species infecting humans [Wikipedia: 'Plasmodium falciparum'], *plasmodium falciparum* is by far the worst (from this point we will refer to *plasmodium falciparum* as malaria).

Accompanied with spiking fever and multiple organ failure, the parasite claims over 2 million lives every year. The most "disturbing" fact in this context is that it is treatable and preventable. Due to lack of resources the disease is still so prominent in the Third World. According to Jeffrey Sachs (director of the UN Millennium Project), there exists a vicious poverty-cycle which is quite effective in spreading the disease. Because of the high childhood mortality rate, there is a reactive high fertility rate in order to maintain the desired number of surviving offspring. In effect, already compromised adults are having many children who grow up in a clinically hostile environment.

Due to growing resistance of the parasite to the low-cost prophylaxes, the concerns are increasing and the use of prophylaxes has been restricted in some areas. Uganda in 2003 had a population of 24.7 million out of which an estimated 9.8 million carried the infection each year [22]. According to the organization Health Politics (www.healthpolitics.org), there have been 1500 reported cases in the United States over the past century. However, 90% of these infections were contracted abroad and another 7% through blood transfusion. From these numbers it is safe to say that there is no problem with malaria in America.

3.2.4 Life Cycle of Malaria

There is a common conception that malaria is generated by mosquitoes, which is partly true, but more correctly, they only serve to carry and serve as a host for sexual reproduction. The female *Anopheles* mosquito is the host providing a comfortable surrounding for the parasite to multiply. Unfortunately, it can fly and it likes to bite humans. Clearly, infection cannot take place if one is not bitten so preventive methods can focus on this aspect. However, if a lasting preventive method targeting the actual parasite could be developed, it would clearly be preferable.

The parasite undergoes two general cycles, an asexual and a sexual. The former takes place inside the human body and the latter inside the mosquito. One would not exist without the other. Inside the mosquito, the parasite exists as a *sporozite* (its infective phase) and assembles in the salivary glands. As the mosquito bites a human, the *sporozites* enter the blood stream and move quickly to the liver,

which seems to be a comfortable place for the parasite to asexually reproduce. Inside the liver cells, one *sporozite* divides into 30-40 000 *merozoites*. Both *sporozites* and *merozoites* are part of an organic family known as the *Apicomplexans*, which carry a special organelle enabling them to penetrate host cells. Once a liver cell cannot hold anymore dividing cells, it bursts and the *merozoites* re-enter the blood stream and target the RBCs. After penetrating an RBC the *merozoite* morphs into a *trophozite* (which is a *merozoite* in its feeding stage) and feeds on the hemoglobin inside the cell. It then undergoes another asexual reproduction phase in the RBC (*erythrocytic shizogony*); dividing itself until the RBC (*erythrocyte*) bursts, the *merozoites* are again released into the blood stream to repeat the asexual reproduction cycle in healthy RBCs. It is at this point where the human host starts noticing the symptoms for the first time with acute fever and chills. These repeat every 2-3 days, as this is the time it takes for the *erythrocytic shizogony* to complete. After a couple of cycles, some *merozoites* develop into gender specific *gametocytes*, which cannot sexually reproduce in the human host. They travel in the blood stream until another female *Anopheles* mosquito bites the human and both types of *gametocytes* enter the blood stream of the mosquito where sexual reproduction occurs. After a couple reproductive steps inside the mosquito, new *sporozites* are again collected in the salivary glands of the mosquito, ready to enter a new human host, and the cycle is complete (see Fig. 4.3.1-1). [23].

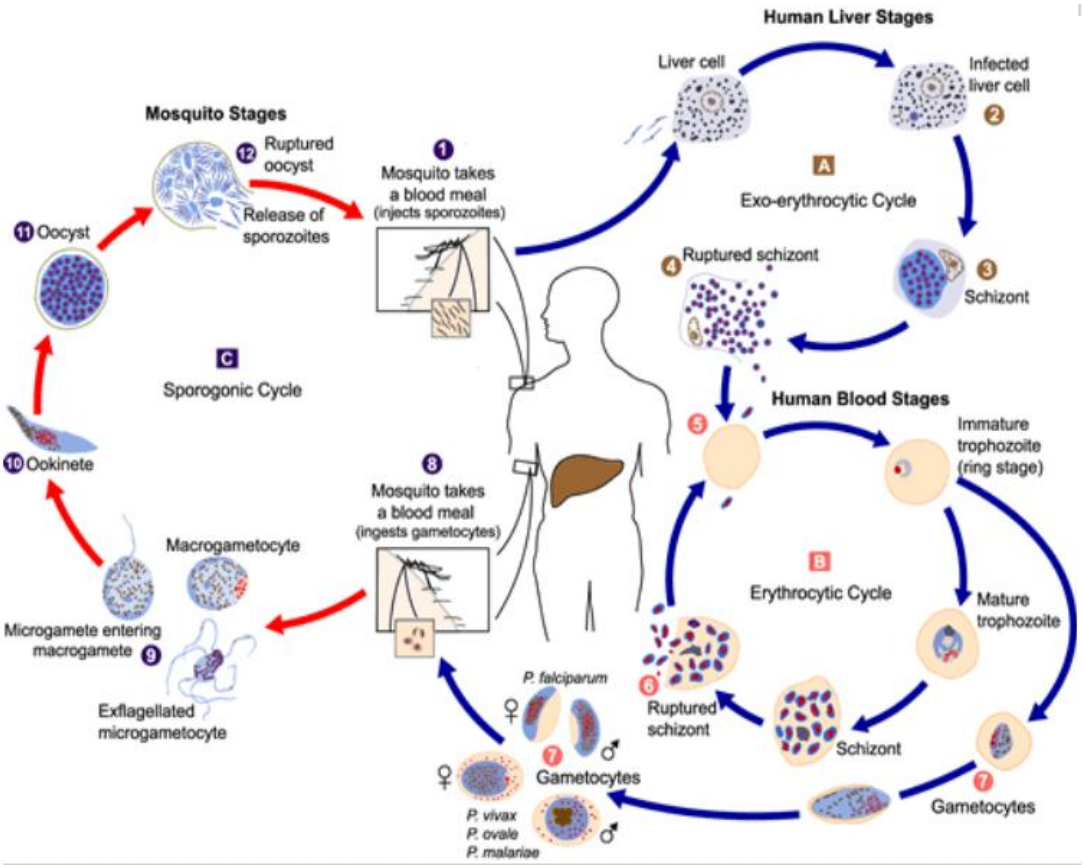

Fig. 4.3.1-1. The malaria life cycle in the *Anopheles* female mosquito as well as in a human. [Centers for Disease Control website]

Instrumentation

This section will provide a relevant, yet brief description of the machined and optical components that are of specific interest to this microscope. Since the construction of the microscope was one of the primary purposes of this project, significant time will be spent explaining the special components. A Model SP-80 metallurgical microscope from Brunel Microscopes was purchased and removed of its illumination source and electronic circuits. The reason for choosing a metallurgical microscope is that it has capability to illuminate a sample in reflection. The microscope was then modified according to Fig. 4-1.

4 Microscope Overview

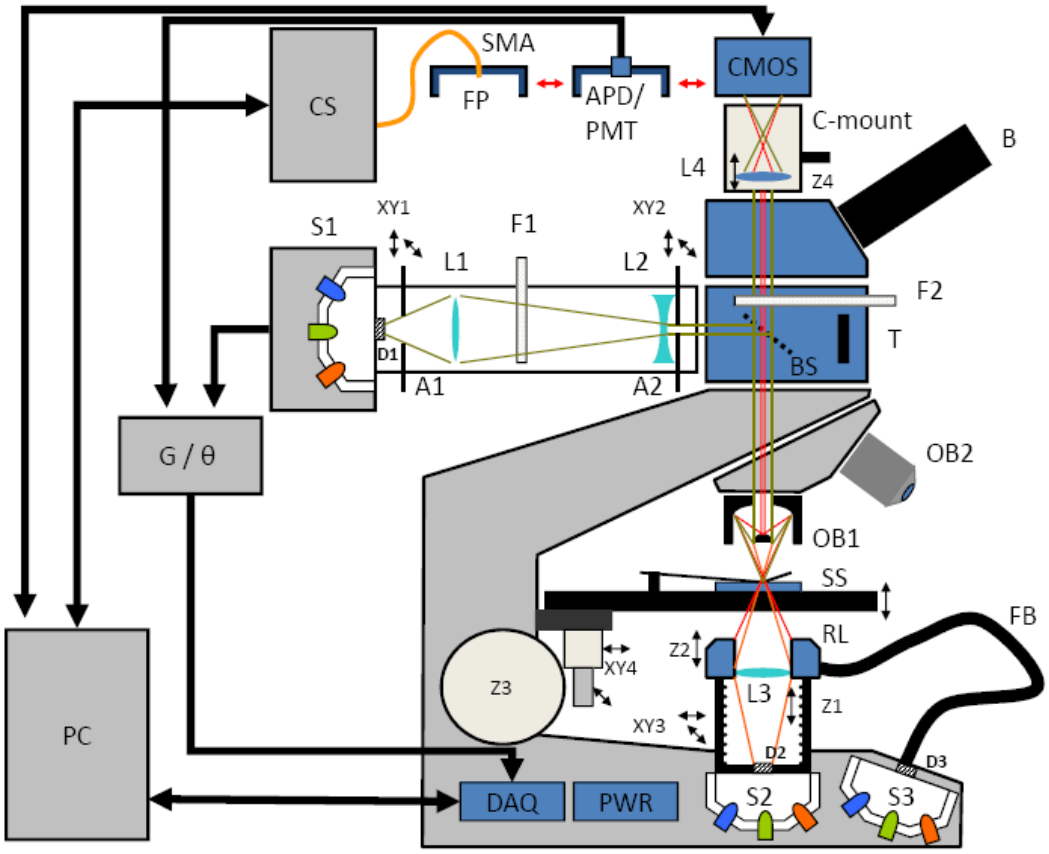

Fig. 4-1. A detailed description of all the components inside as well as outside the microscope used to fully operate it. The only information lacking is the detailed electronics which will be covered in Appendix I. [24]

4.1 Machined Components

The microscope was adapted to propagate light using a number of mechanically manufactured parts. Depending on how the light is supposed to be controlled, different materials were used. Cost was also a determining factor when

deciding which material to use. Teflon was used for parts where light needed to be confined due to the relatively high diffuse reflectance of Teflon. Some consideration was put towards using a material called Spectralon (99.9% diffuse reflection); however, the cost of the material alone was unrealistic. For the parts where it was desired to have light absorbed, black Delrin was used, which is some sort of soft, easily formable plastic. In total eight components were made. A brief description will be given of the ones with more importance.

4.1.1 LED holders

The components of most significance are the ones holding the LEDs. 9 separate LED housings contain a total of 13 LED chips (including 1 triple and 2 double). The LED holders were designed so that as the LEDs are inserted, their optical axes strike one and the same point. The holes for the LEDs are arranged so that one hole in the center is evenly surrounded by 8 holes. In order for the surrounding holes to aim at the same point as the center hole, they need to be angled towards the center and displaced a distance from the center. Figs. 4.1.1-1 and 4.1.1-2 show how the holes are arranged.

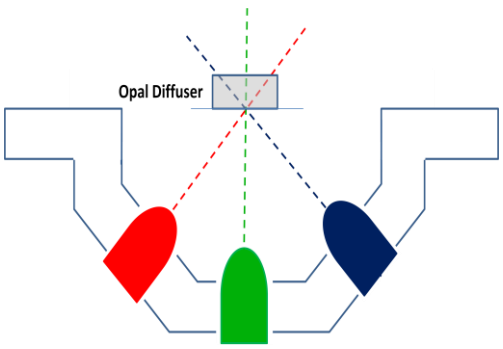

Fig. 4.1.1-1. Cross sectional view of LED holder where the optical axes of the LEDs strike one and the same point in which the opal diffuser lies.

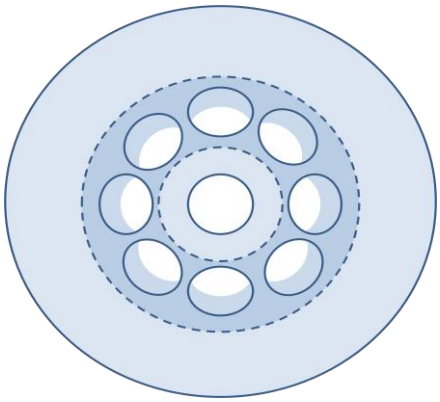

Fig. 4.1.1-2. Bottom view of LED holder showing the arrangement of holes where one hole in middle is symmetrically surrounded by 8 holes.

Some of the LEDs contain more than one chip which do not lie at the exact center of the housing. This causes the optical axes of some LEDs not to strike the desired point exactly. Since the problem is greatest with the tri-chipped LED, it is placed in the center to minimize the error. At the common aiming point there is an opal diffuser which functions to spread the incoming light. The resulting distribution can be estimated to be Lambertian, which means it spreads the light evenly in all directions. The intensity distribution obeys Eq. 4.1.1-1

$$I = I_{max}\, cos^{m}(\theta) \qquad \text{(Eq. 4.1.1-1)}$$

Where m>1 and represents how much the illumination diverges from the central axis. If m is higher, the illumination lobe will be more elongated in the direction of propagation.

It is illustrated in Fig. 4.1.1-3. According to the Eq. 4.1.1-1, at 60° divergence from the optical axis, 50% of the maximum light intensity will be measured. Similarly, at 90° no light should be measured. The reason for using an opal diffuser is to remove the dependency of the position in the LED holder. A major drawback is that almost 50% of the light is lost due to the highly reflective surface of the opal diffuser. With a ground glass diffuser more light will pass through, but the light distribution will not be even therefore making it more dependent on the direction of the incoming light.

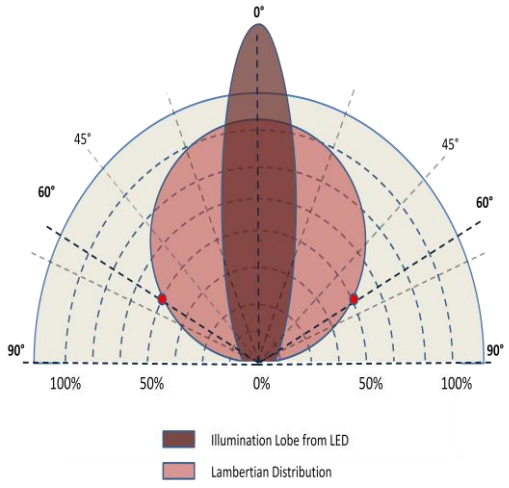

Fig. 4.1.1-3 Lambertian distribution vs. LED distribution of light. Note that at 60° divergence from the center axis, the light intensity will be 50% of the max intensity. At 90°, no light is seen.

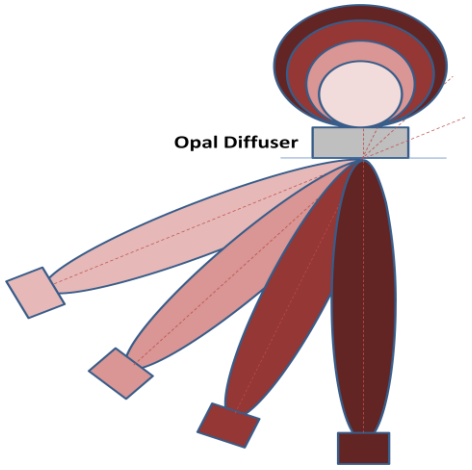

Fig. 4.1.1-4. Effect of tilting LED with respect to normal. In reality the emission lobes from the diffuser will be of equal size but with varying intensity. It is more a descriptive figure than exact.

The distance from the center and the inclination angle are interdependent and can be chosen arbitrarily where a larger angle requires a greater distance from the center. However, considering the LED illumination lobes, it is of interest to keep the angle as low as possible See Fig. 4.1.1-4. According to Fresnel equations light of normal incidence will have a power reflection of approximately 4% when passing between air (RI≈1) and glass (RI≈1.5). At higher angles, more of the intensity will be reflected; therefore it is inefficient to illuminate the diffuser at larger angles. Ideally, all illumination sources would emit from the exact same position. Therefore it is of much interest to have as few factors change from source to source. Using a larger angle also requires the holes to be placed further down from the common point in order to fit into the limted space.

For each illumination mode there is an almost identical LED holder. The only difference between them are the shapes of the edges since they attach to different parts of the microscope.

4.1.2 Bright Field

Connecting with the LED holder in bright field mode is the component shown in Fig. 4.1.2-1. Drawn in the figure is the complete assembly which propagates the bright field illumination. The ‘Brass Tube’ and ‘plastic Top-Hat’ were mechanically

customized to fit together with the LED holder, microscope base, and the fiber ring light (discussed shortly). The 'Brass Tube' serves to adjust the length between the diffuser and the lens. This changes the magnification as well as the distance to focus (according to Eqs 1-1 and 1-2). It also adjusts the angle at which light falls on the sample in the dark field mode, which will be discussed further shortly. The 'Top Hat' is made from black Delrin since any light that strikes the surface should be absorbed. The tube is made from brass which has been chemically treated in order to remove its reflective surface. The reason for not wanting any reflection off the sides is that this will provide 'uncontrolled' light in the experiment. If all the light from the diffuser managed to pass to the lens without reflecting off the walls of the 'top hat', the beam profile would only be limited by diffraction and the PSF of the lens. This is not impossible, but very hard to do, so the resulting image will have a weak halo due to unwanted reflections along the way. To minimize the reflections, the inside wall of the tube was made with a groove spiraling from the top to the bottom. This creates a less smooth surface and makes it harder for the reflected light to make it out, as can be understood from the discussion about scattering in section 1.5. See Fig. 4.1.2-2

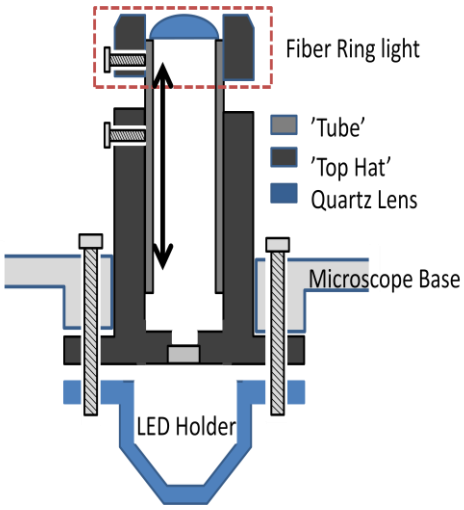

Fig. 4.1.2-2 A close up view of how the grooved inner surface backscatters the light striking the wall. The efficiency is not close to 100%, but it decreases the PSF to at least some extent.

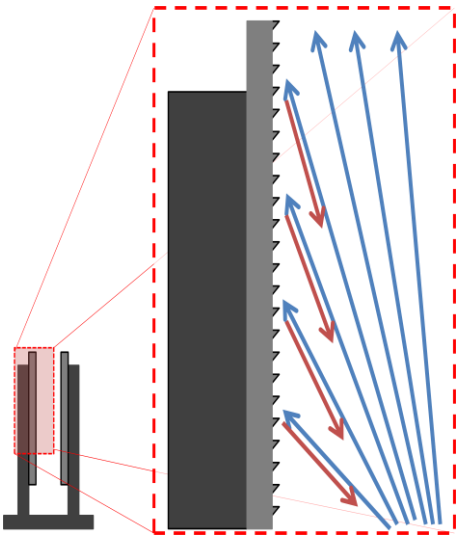

Fig. 4.1.2-1 A cross-sectional view of the part propagating the transmission illumination. The fiber ring light can be adjusted vertically changing the angle at which the sample is illuminated. This also changes the magnification and focal distance of the transmission mode illumination.

The pieces discussed above were the ones given most consideration during design. The remaining pieces serve to adapt optical components or cables to the microscope mounts. The dark field illumination comes without much modification from the fiber ring light (discussed as a separate component below). The only custom made pieces for this illumination mode were the brass tube recently discussed, and an adaptor to the LED holder. Similarly for reflection, the LED holder was designed to fit onto the microscope. The CMOS camera attaches to the microscope by a C-mount connector.

A plastic piece was customized to mount onto the microscope on one end, and having an SMA connector on the other one so that a fibre can be connected. The plane in which the fiber aperture lies is the same as where the image-chip of the CMOS camera lies in relation to the sample to better relate signal intensities between imaging and point-monitoring. The camera specifications are discussed in more detail below.

4.2 Optical Components

This section will spend some time describing the optical components that bear some significant importance for this microscope. The function of basic optical components such as lenses can be explained by Eqs 1-1 and 1-2 and do not need to be covered any further. The purpose is to present the function of the components not generally encountered in optical systems as well as the motivation for using them.

4.2.1 Fiber Ring Light

The fiber ring light (FRL) consists of several fibers bundled together and guided from a glass-polished end-face into anodized, aluminium housing where it emits diffuse light in 360° around the central axis. Due to the plurality of fibers, the housing emits shadow-free light since each fiber contributes to the illumination and creates rather even light. According to the specifications of the FRL the beam exit-angle is 37°, but it is important to remember that it has been optimized for this angle meaning that the highest intensity is found here. In reality there is some form of distribution which has not been experimentally determined; however, the sensitivity of the objective in conjunction with the emission from the FRL has been measured and will be presented in the 'Measurements & Results' section. Fig. 4.2.1-1 shows how the FRL emits light.

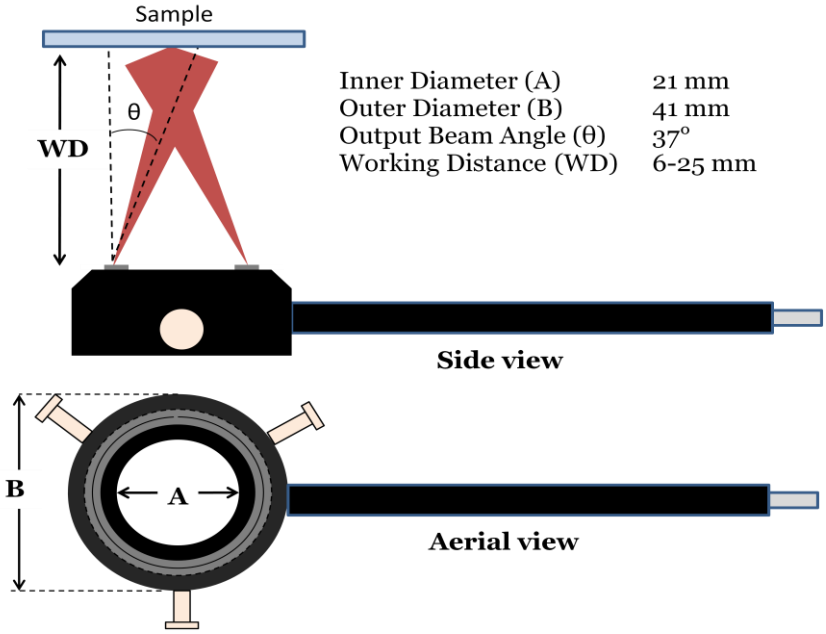

Fig. 4.2.1-1. Side and aerial view of the FRL. The most imporant specifications are given in the image. Note, the figure doesn't properly illustrate the beam profile of the emerging light.

4.2.2 Reflx™ Objective

As the name implies, the Reflx™ objective is based on reflective rather than dispersive optics. Upon reflection, part of the wave is reflected and the other refracted according to Fresnel's equations. In a reflective objective only the reflected part of the waves will reach the imager without passing through a medium and is therefore not subject to absorption (beyond that of air, which is assumed to have a refractive index of 1). As we know, absorption and refractive index are causally related through the Kramers-Kronig dispersion relation (Eq. 1.3-1). Since there is no absorption, the reflected portion of the waves will maintain the same phase velocity through the objective, which removes the effects of chromatic aberration. There are of course power losses according to Fresnel's equation which should be kept in mind.

The objective is essentially a miniature form of a Cassegrain telescope working in reverse. A symmetric Cassegrain reflector consists of one parabolic and one hyperbolic mirror aligned along the optical axis with their curved surfaces facing each. Fig 4.2.2-1 shows a cross-sectional view of the Reflx™.

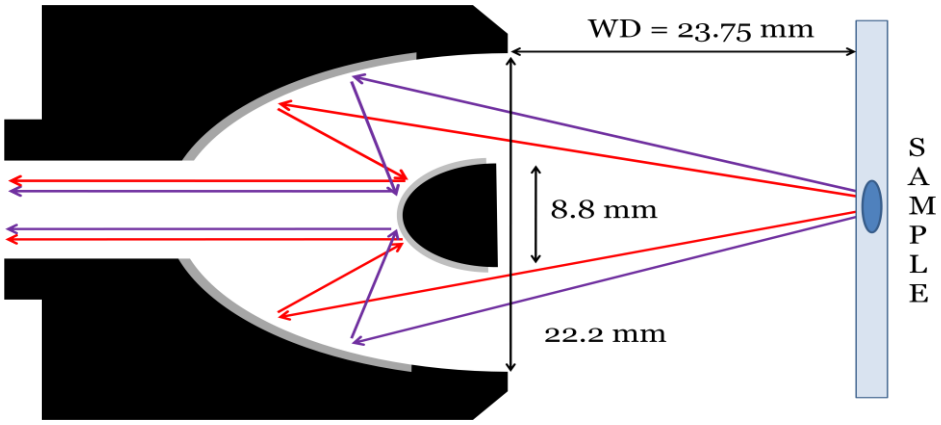

Fig. 4.2.2-1. Cross-sectional view of the reflective objective. Both red and blue light obtain magnification through reflection and no chromatic aberration occur. The specifications drawn in the image will be used for calculating the detection regions of the objective in order to properly define the sensitivity lobes for each geometry. The figure is not drawn to scale to the objective, neither are the arrows drawn in accordance with the law of reflection.

One drawback with this design, which can be seen in the figure, is that the parabolic mirror needs to rest in the center which means part of the angular spread of the sample will be automatically blocked. Unfortunately, this region is what mainly defines transmission, or at least all of what is defined as collimated transmission. Luckily, transmission is the mode in which the strongest illumination can be obtained so an image with good contrast can still be seen. During the design/test phase this was one of the main issues addressed. Considerations were made to use the FRL to illuminate the sample in transmission and having a beam focused on the dark spot of the objective act as scattering illumination. Both actually work and will be shown in the 'Measurements & Results' section.

4.2.3 Polka-Dot Beam splitter

In order to implement reflection measurements the light needs to illuminate the sample from the same direction in which it is detected, so a beam splitter is used. Since much effort was put towards creating an instrument minimal chromatic aberration over the spectral range (375 nm – 940 nm), some effort was put into finding a beam splitter which could do just this. A polka-dot beam splitter is simply an array of holes and mirrors which effectively results in half of the area being open where 100% of the light passes and half being a mirror reflecting 100% of the incoming light (Fig. 4.2.3-1). Since a beam splitter is optimized to transmit in a relatively narrow spectral region, it is of interest to account for this in the microscope. Using a polka-dot beam splitter allows for a very even transmittance over a wide spectral region, but some issues still arose and will be covered in the 'Discussion' section.

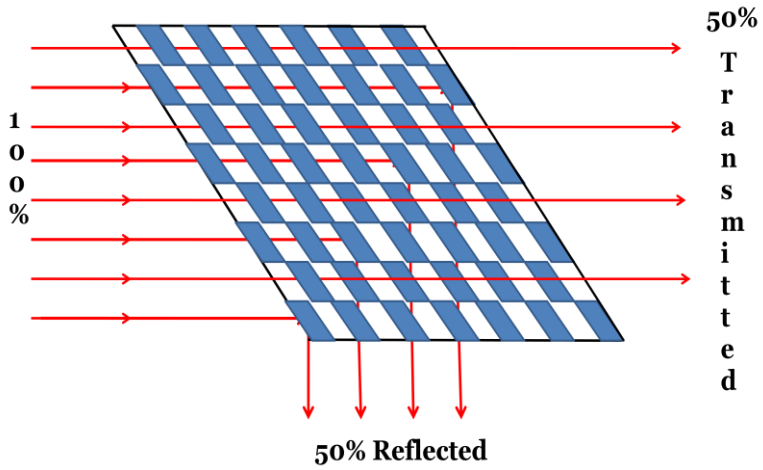

Fig. 4.2.3-1. The polka-dot beam splitter transmitting 50% and reflecting 50% of the incoming light. Different ratios can be obtained by simply changing the effective surface of holes and mirrors.

4.3 Detector

Some discussion should be given around the choice of camera. Since the illumination is spectrally resolved, it is only necessary to get a monochromatic camera. The camera used is a Model AVT Guppy 503-B/C. It has a 12-bit image-depth and an imaging chip consisting of 2592x1944 pixels each having a size of 2.2 x 2.2µm.

4.3.1 Dynamic Range

The dynamic range is characterized by the cameras bit-depth, which is the ability of the camera to resolve various light intensities; its ability to convert the analogue signal to a digital signal on the computer. The camera is essentially a sophisticated Analogue-to-Digital converter for light intensity signals. A 12-bit monochromatic camera can discretize between 2^{12}=4096 light intensities between

'zero light' and saturation. This assumes that the signal is not too weak and drowned in noise. The signal-to-noise ratio (SNR) of the signal limits the intensity resolution.

4.3.2 Physical Dimensions of Imaging Chip

The effective image chip size is 5.7 x 4.3 mm. In this region an array of approximately 5 million (2592 x 1944) square pixels of 2.2 x 2.2 μm exist. Depending on the magnification provided by the entire system, the field-of-view (FOV) will vary. In either case, the FOV will be imaged onto the entire chip. If the system provides a magnification of 15x (as the reflex objective does) and RBCs with diameter of approx. 8 μm are imaged, the camera will be able to image roughly 50 tightly packed RBCs horizontally. This means that each blood cell is, at its center, spanned by about 50 pixels each being able to produce a unique spectrum from UV-IR. Since the RBC is 8 μm in reality, the combination of the magnifying optics and small pixel-sizes of the camera allows for a spatial resolution of 8 μm/50 = 160 nm. However, making calculations like this is unrealistic without considering the PSF of the optics between the object and imager since this will be the final limitation of what information can be extracted [15]. There are easy ways to measure this which gives much more reliability when communicating a result.

4.3.3 Shutter Modes

The shutter operation is handled by two separate registers inside the camera: the time-base and the relative shutter. The absolute exposure time is simply the product between the two. This model can operate in two shutter modes, Electronic Rolling Shutter (ERS) and Global Reset Release (GRR). This is unique to the CMOS model and should be understood because improper use can alter data as will be discussed. In ERS-mode each row is 'turned on' for the same amount of time but each starting with a little delay from the previous. The result gives a uniform exposure of the entire sample, but if there is any movement during capture, it will distort the image. In GRR-mode all rows start exposure the same time but end at successively later times for each descending row. This causes the image to be brighter towards the bottom, but it takes care of the problem of moving objects. To overcome the imbalanced brightness special lighting could be used or an extra mechanical shutter [AVT Guppy Techman Manual]. The maximum exposure time possible for this model is 2.3 s.

4.4 Light Emitting Diodes (LEDs)

The use of LEDs is exponentially growing for commercial products as well as for research where new applications are discovered on a daily basis. The reason for having such a huge market impact lies in the fact that the manufacturing costs are essentially zero compared to their effective output.

Due to the significant use of LEDs in the microscope some pages will be spent explaining optoelectronic properties of the LED so that useful information can be extracted from their characteristics.

The difference between a light-emitting diode and an incandescent bulb mainly lies in how the light is generated. In a light bulb there is a filament connected between anode and cathode which emits thermal radiation when current is passed through. Anything that has some thermal activity (almost everything) will emit thermal radiation. The peak wavelength (λ_{max}) measured in meters (m) will depend on the temperature (T) measured in Kelvin (K) of the object and the relation is explained with Wien's displacement law (Eq. 4.4-1),

$$\lambda_{max} = \frac{2.8979685\ x\ 10^{-3}[m \cdot K]}{T} \qquad \text{(Eq. 4.4-1)}$$

Light-emitting diodes consist of two semiconductor materials separated by an insulating region, called the depletion region. The materials are chosen so that one has an excess of electrons (n-type material) and the other an excess of holes (p-type material). The absence of an electron is referred to as a hole for conventional purposes. A molecule which is ready to accept an electron is said to have a 'hole' (in this context). Naturally, electrons and holes want to recombine and release energy, therefore these two types of materials are combined along with an insulating material between so that this recombination cannot naturally occur. The energy released through the recombination can either occur through a radiative (photon emitted) or non-radiative process and the probability is determined by the internal quantum efficiency (η_i) [5].

Photons are always spontaneously emitted from a semiconductor due to what is called thermal noise. As particles heat up they gain energy and start to move more violently. With enough energy to clear the insulation region (also referred to as the bandgap or depletion region) a single photon is released. A few photons here and there is not enough to have any significant light output, so in order to achieve that, recombinations should occur in a spatially confined region where the concentration of both electrons and holes is high on opposite sides of the bandgap. This happens when there is an externally applied forward bias and the charge-carriers are drawn to their respective regions of interest according to Fig. 4.4-1.

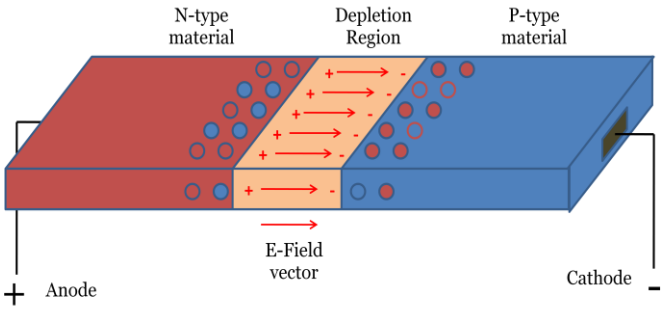

Fig. 4.4-1. As a forward biased external voltage is applied, an electric field across the depletion region as indicated arises. Eventually, the applied voltage is so large that electrons start jumping across the depletion region in the direction of the E-field, recombining with holes and releasing energy.

The external voltage gives rise to an electric field across the depletion region. The negatively charged electrons are drawn towards the positive side of the depletion and the positively charged holes are drawn to the negative side of the depletion

region. As the charge-carriers have been spatially confined, infinitely more recombinations can occur now and give rise to very intense emission. The wavelength of the emitted light is in a direct relation to the energy required to clear the bandgap according to Eq. 4.4-2

$$E = \frac{hc}{\lambda} \qquad \text{(Eq. 4.4-2)}$$

Where h is Planck's constant and c the speed of light in vacuum

If E is measured in electron volts (eV) and λ_{max} in (nm), the formula can be simplified to $E = 1240\, nm \cdot eV/\lambda$. This equation is quite useful for determining which wavelength an LED emits when only a multimeter is at hand, which will be demonstrated.

4.4.1 I-V Response of LED and Emissive Yield

An LED can be considered a forward biased pn-junction where energy is released through photons. Applying an external reversed bias causes the process to change where a potential is instead built up in the opposite direction. Since the potential is pulling the electrons and holes in the opposite direction they naturally want to flow, no recombinations occur across the depletion region. Instead, whenever a photon carrying matching energy of the bandgap strikes the semiconductor, the energy is deposited in the valence band where an electron gains enough energy to jump into the valence band and creating a hole behind, in a process called *generation*. The electron and the hole will now move in opposite directions in their respective bands and give rise to a current (if there is a connected circuit). The current measured is directly proportional to the light intensity.

The I-V response of any electrical component is useful to reveal its behavior in a circuit. It is obtained by measuring the current through a component as a function of the voltage applied across it. Ohm's Law (V=IR) is the I-V response of a resistor, for example. As discussed, an LED will emit light when forward biased, and give rise to current (under the conditions provided above) if reverse biased. These characteristics are illustrated in Fig. 4.4.1-1.

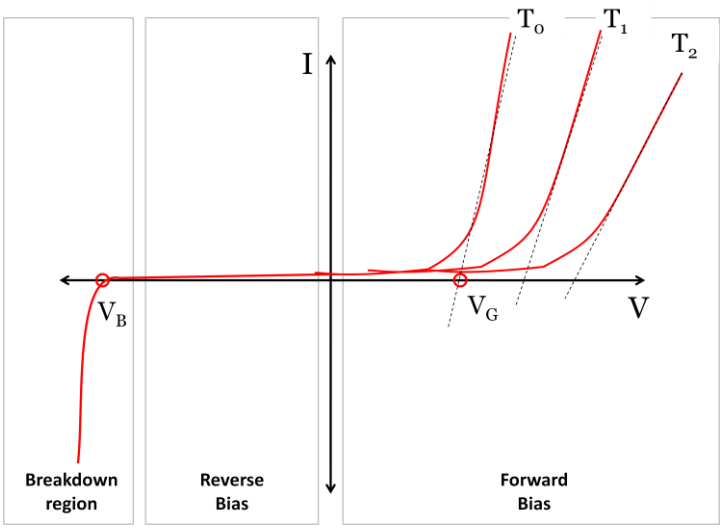

Fig. 4.4.1-1. I-V characteristics diagram for an LED. The extrapolated lines represent the bandgap energy, V_G. T_0 is the temperature of normal operation. T_1-T_3 represents the LEDs behaviour as the thermal activity changes. If enough reverse bias is applied, the insulating region will eventually break and current will flow in reverse. This occurs at V_B

Whenever the applied voltage (V) is positive, there is a current. But the LED seems to exhibit an interesting behavior in the beginning where no current is measured as the voltage is increased. This is the region where the electrons are given energy, but not enough so they can clear the bandgap of the semiconductor and emit light. Once sufficient energy is supplied, electrons and holes start recombining and current flows. If all electrons and holes available in the conduction and valence band respectively were at the border of the depletion region without any thermal activity, they would all recombine at the instant the energy supplied matched the bandgap. The result would be a horizontal line from $0 < V < V_G$ at I=0, then a vertical line from $0 < I < I_{max}$ at $V=V_G$. There is of course no such thing because electrons and holes exist throughout their entire respective regions, and due to thermal activity, they will already carry some energy. Therefore there will be a slope as well as a lateral shift which is an indicator of the internal resistance, which can be used to find the temperature of the LED. Extrapolating this line to the V-axis therefore yields the bandgap energy at the point the extrapolation intersects I=0. The slope of this line is an indication of thermal activity. A smaller slope is an indication of a higher thermal activity inside the LED. The photons released through recombination will have wavelengths according to Eq. 4.4-2. If a wider range of energies undergo recombination, the emission becomes spectrally broadened. Also, with increased thermal activity, more spontaneous recombinations occur leading to more uncontrolled processes in which no radiation is emitted. Therefore, as the temperature increases, not only does the spectral resolution decrease, but the overall emissive yield decreases.

Measurements & Results

This section will present the results obtained from measurements as well as theoretical calculations predicting certain outcomes of the instrument performance. First, the calculations and measurements with regard to the sensitivity lobes of the angular geometries will be presented and compared. Then, some results with regard to malaria detection will be shown and a preliminary contrast function will be constructed. Finally, measurements of the spectral bands taken with a spectrometer will be presented to reference the data taken of the RBCs.

The amount of raw data collected is quite extensive, from which much analysis could be done. However, within the context of this project, only preliminary spectral characterization of healthy and infected blood cells will be presented in order to lay the foundation of coming work. This is also because the system has not been properly calibrated yet; however, some data will be shown which indicate that the system is working quite well. Analysis of the developmental stages will not be covered here, nor will any statistical models be made at this point.

5.1 Polar Maps and How They are Constructed

Polar maps are useful to represent an angular distribution of scattered photons off a sample. In a polar map the outgoing direction of the photon is compared to its incoming direction. Arbitrary to what incoming angle it has, it has either been deflected or not. This is therefore a measure of how much a photon has deflected from its initial trajectory. Suppose two photons, from two different directions interact with a sample where neither is scattered off the sample and continues in the same trajectory it had. Both these photons will be accounted for the same way and will be plotted in the same sector of the polar map. The reason for applying this representation technique to our instrument is because two important components (the fiber ring light (FRL) and the objective) emit and detect photons from several angular regions (See Fig. 4.2.1-1 and Fig. 4.2.2-1). To remove the directionality variable, we can simply compare the angle of deflection to the angle of incidence instead of comparing both these angles to the optical axis. It becomes much easier to define what scattering, transmittance, and reflectance are. It can be compared to the discussion in Sect. 2.7 on references, where we have now removed some variables by normalizing the photon to itself. It no longer matters from which point in the angular plane of the FRL the photons emerge, as well as in which part of the objective it enters. All that is of interest is how much a photon has been deflected from its initial trajectory. Thus, if we consider the optical axis to be normal to the object plane and know both the angle at which the photon strikes the sample as well as the angle through which it can detect a signal, we can easily calculate which deflection angles a photon should have in order to be detected as scattering, reflectance or transmittance. Using the information from Fig. 4.2.1-1 and Fig. 4.2.2-1, these angles can be calculated but first some approximations should be made.

5.1.1 Sensitivity Regions in Polar Maps

As discussed in Sect. 1.1 (Basic Optics Theory), light cannot be properly described by drawing arrows, but a good approximation can be made as long as the reasoning behind making it is acceptable. We are going to apply some approximations to the emission distribution of the FRL. According to the manufacturer specifications of the FRL, the beam exit angle is 37°. This does not mean that all of the light will be seen at this angle, but rather the highest intensity will be measured here. There will be some form of distribution of light depending on a number of things inside the FRL, which is not of interest for our approximation. The reasoning behind approximating the FRL emission as an arrow comes from the fact that the field of view (FOV) at full resolution is approximately 1 mm wide (measured). In its closest position, the FRL is about 20mm below the sample and the distance from where the light emerges to the optical axis is 11 mm. This means that in its highest position (where angular emission variations across the sample will be of most significance) the exit beam angle from the FRL can only vary approximately 1° across the FOV. Therefore, intensity variations can be neglected over this region and

an arrow at 37° can be approximated for calculations. The angular sensitivity regions were calculated and are shown in Figs 5.1.1-1, 5.1.1-2, and 5.1.1-3

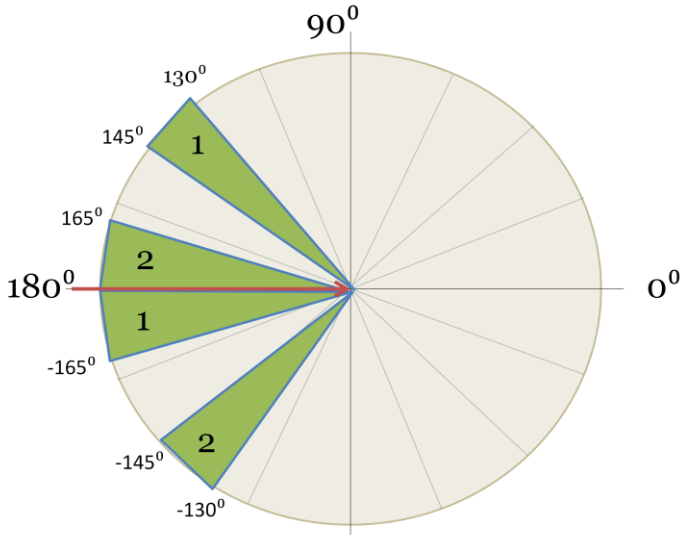

Fig. 5.1.1-1. The angular sensitivity region for reflectance measurements. One important thing to keep in mind, which is illustrated in Fig. 3.1.3-1 is that photons can emerge from both sides of the objective aperture and either be detected directly across which results in a deflection of 50° (twice the maximum detection region of the objective) or it can be deflected straight back where it came from which results in a deflection of 180°. These angles are deflection maxima and since the objective detects over a 15° region, they appear as they do in the image. In a cross-sectional view of the objective (Fig. 4.2.2-1) we can assume there are 2 regions from which a photon can emerge. These are indicated with '1' and '2' in the figure so we can see that each outgoing photon can be detected in two regions.

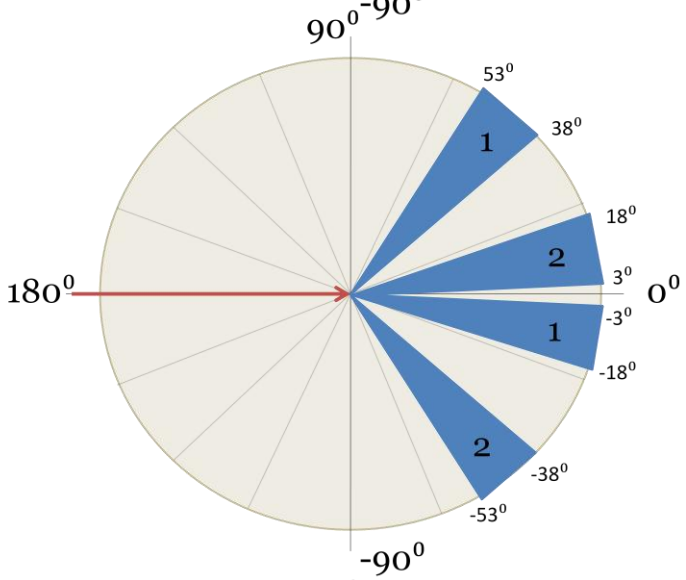

Fig. 5.1.1-2 The angular sensitivity region for scattering measurements. Similar to the reflectance lobes, the scattering has two sets of sensitivity sectors indicated with the numbers. The sensitivity regions for reflectance will not change as long as the working distance does not change, which can be understood since they detect and emit from the same place. Light emerging from the FRL, however, will depend on how high the sample is placed over the plane from which the photons emerge. We have already concluded that they have an exit angle around 37° which can be approximated with an arrow. With basic trigonometry it is understood that the angle of the incident photon will depend on the height of the FRL in relation to the sample. This will be demonstrated below. For angles indicated, the distance from the FRL to the sample was 22.5 mm.

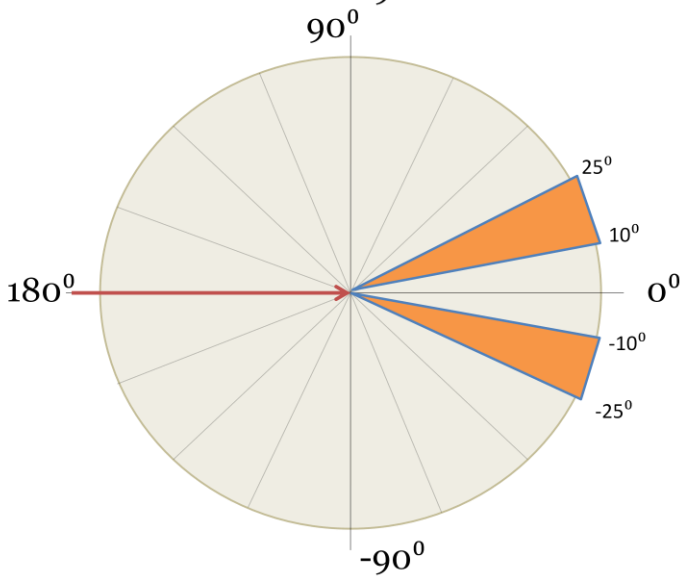

Fig. 2.1.1-3. The angular sensitivity region for transmittance measurements. All photons that are deflected between 10° and 25° from their initial trajectory will be measured as transmission and the illumination will produce a bright field image. In contrast to scattering and reflectance, transmittance only has two detection regions and this is because all light comes from one general direction. Although, this is also an approximation to a certain degree since the light from the center is not an arrow and the size of the beam profile in the detection plane will behave in general accordance with Eq. 1-1 and Eq. 1-2.

Figs 5.1.1-1, 5.1.1-2, and 5.1.1-3 define quite specifically where the sensitivity regions of the different angular geometries are and if they are compared to each other, we see that there are some regions where the definitions overlap. These regions belong to the scattering and transmission mode. See Fig. 5.1.1-4 for all geometries combined. The regions where the sectors overlap are marked with red.

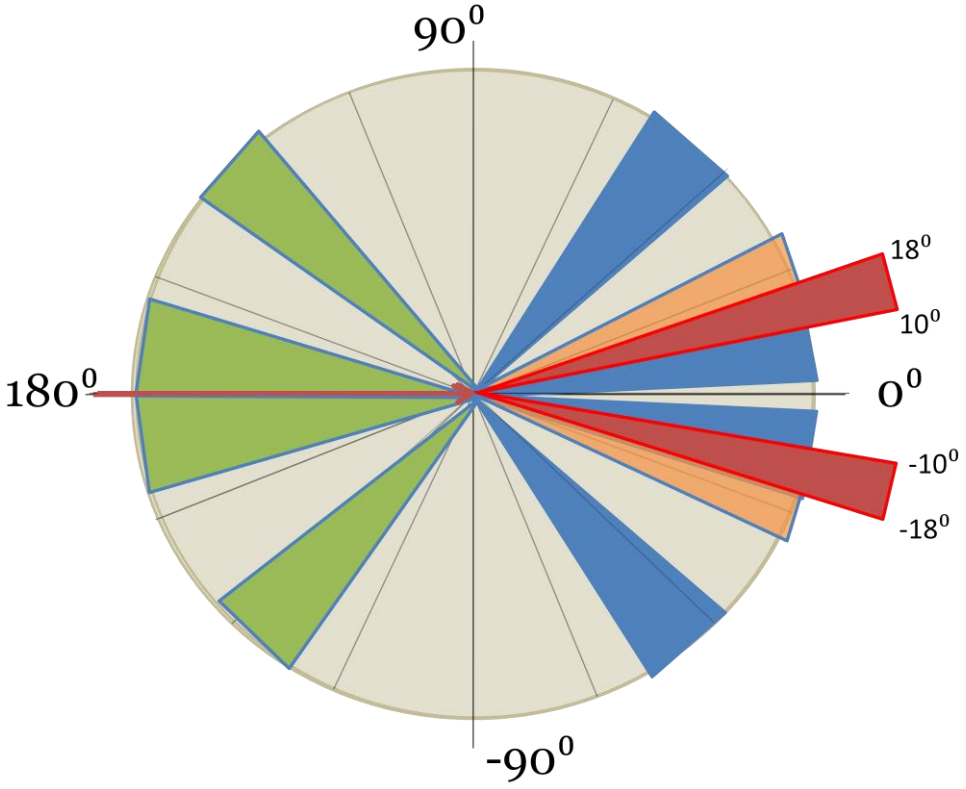

Fig. 5.1.1-4. All sensitivity regions plotted on the same polar map. The assembly holding the FRL and providing transmission illumination was placed at a height of 22.5 which then creates a region of 8° in which both photons defined for scattering and photons defined for transmittance are detected.

In order to not 'count' one photon for two separate modes, the sectors should lie in unique regions and should be lying border to border. As the assembly is lowered, the sectors for the FRL will be drawn together and as it is raised, they will move apart. To study the behaviour of these two modes, one image in each mode was captured at different heights. These results will be presented further below, but first we will present our reasoning of how the light should behave.

At a low position the distance to the sample from the FRL is long causing the angle at which the photon is incident on the sample to be small. In this case, light from the FRL, in the absence of a sample, go straight into the objective. In the presence of a sample, light will either be absorbed and attenuating the signal, or it will be scattered and not detected; this is what we defined as bright field in section 3.1.1.

The light emerging from the center of the assembly (we will call this light 'center light' from now on) will generally behave according to Eq. 1-1 and 1-2 (The lens formula is valid under the assumption that the lens is infinitely thin and the light is infinitely planar and parallel to the lens). The lens that is used has a focal

length (FL) of 30 mm. This FL was chosen so that the focus would be in between the sample and the objective (the thinking behind this was so that objectives of different WDs could be used since the stage can only be scanned through a certain height). As the assembly is successively raised within its capable range, the focus will remain more or less in the same position but the magnification will change significantly. When the assembly is at a long distance from the sample, the magnification will be greater than 1, which means the focused image will be larger than the source (it will create an image of the 5 mm diameter opal diffuser from which the light emerges at the bottom, but with a magnification according to Eq. 1-2). When the assembly is close to the sample, the magnification will be less than 1. From this reasoning, we assume that the center light will provide bright field images only when it is far from the sample, since the magnified image of the diffuser is larger than the objective's blind spot. As the assembly is raised, it will provide dark field images since the light will be blocked by the blind spot of the objective.

The picture series in Fig. 5.1.1-5 shows the two images taken from the two sources, as well as a polar sensitivity map for the FRL. We decided not to include the sensitivity map for the center light since it does not exhibit equally strong angular behaviour with height as the FRL does.

FRL Polar Sensitivity Map Image from FRL Image from center light

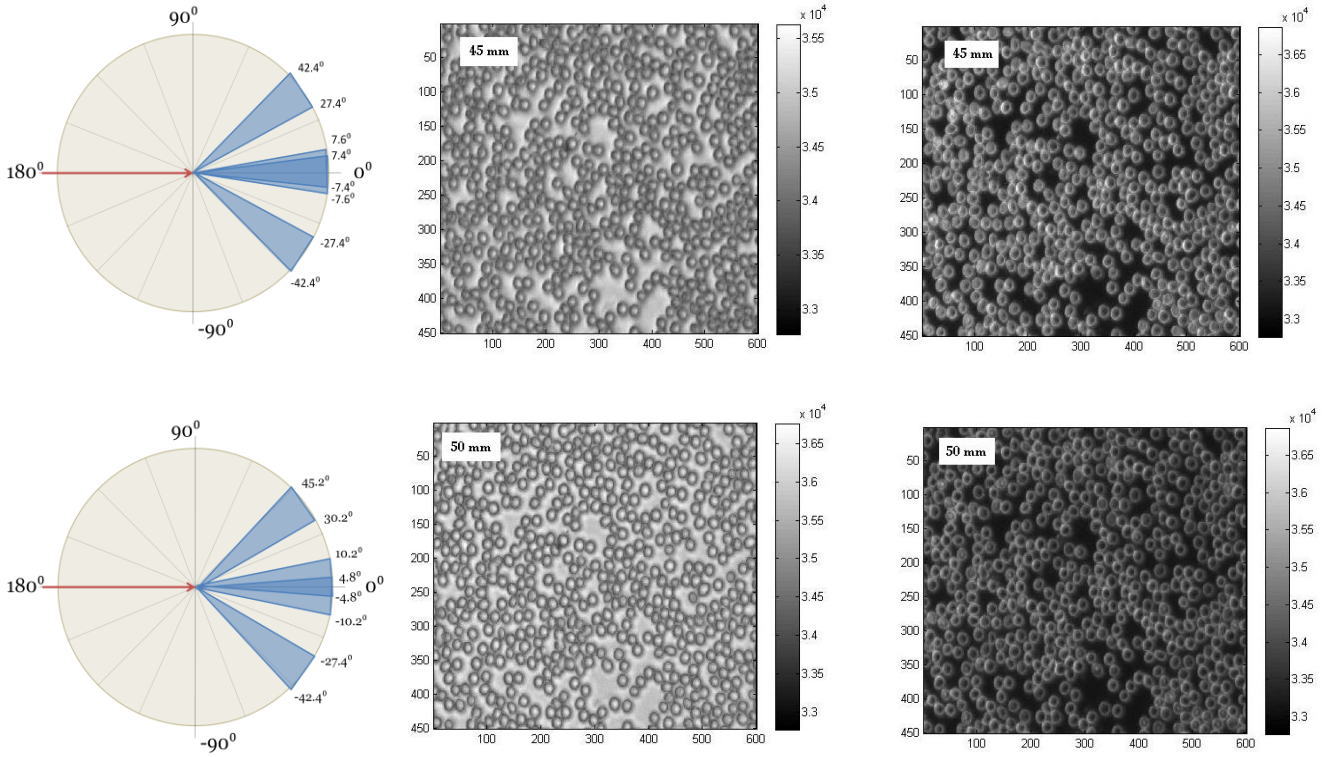

FRL Polar Sensitivity Map Image from FRL Image from center light

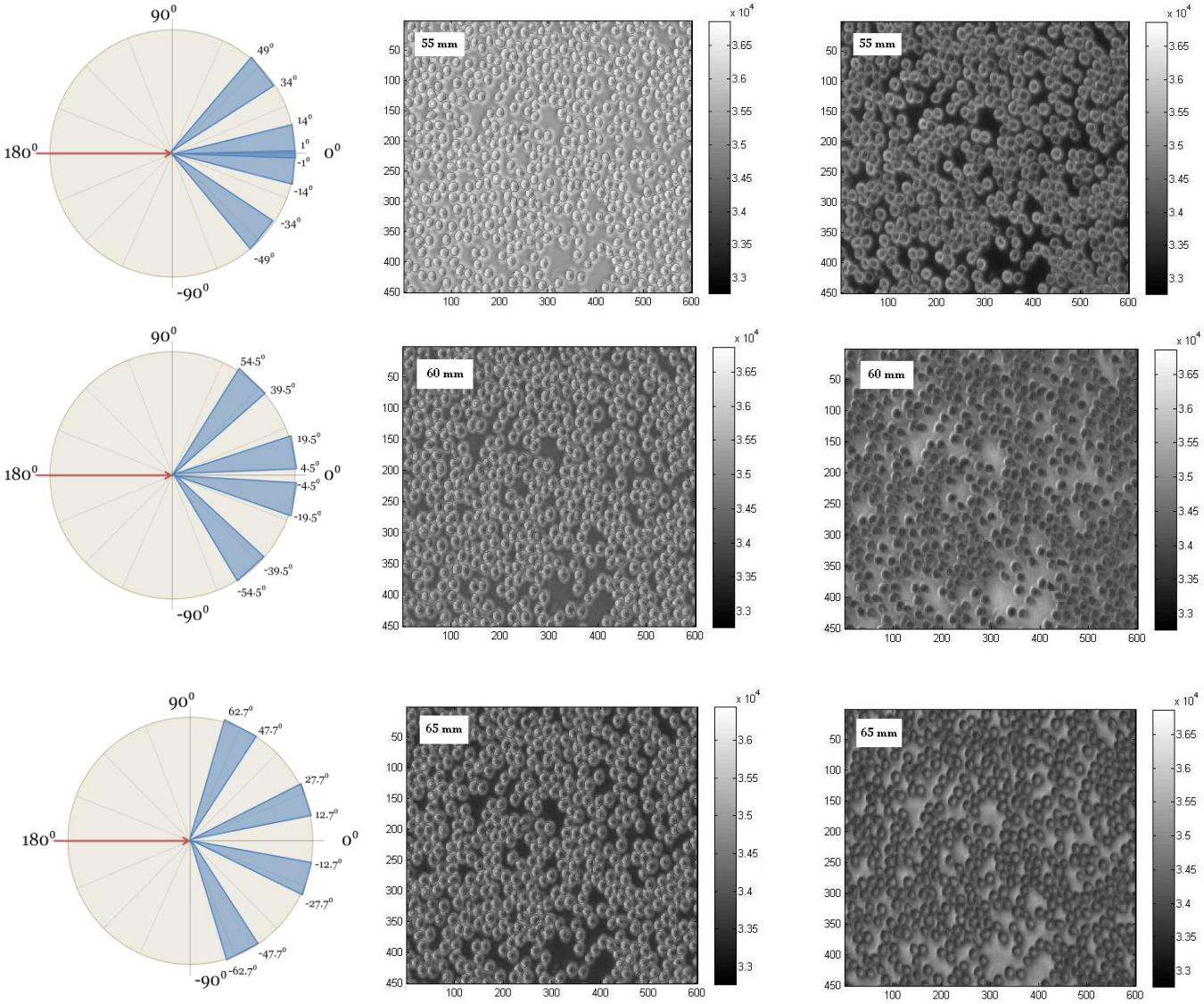

Fig. 5.1.1-5. A picture series of both scattering and transmission mode taken at different heights. Also included are the polar maps for the FRL, which are more affected as the height of the assembly changes.

The picture series in Fig. 5.1.1-5 shows a very interesting result which differs from our expectations with regards to the center light. As the assembly is raised the two modes for bright field and darkfield seem to slowly shift. The angular sensitivity of the FRL can actually be calculated quite well as we can see in the polar maps. As soon as the sectors no longer overlap, the images the FRL produces switch from bright field to dark field. It makes complete sense because as we can see in the polar map, only deflected photons will be measured. However, the center light provides a dark field image at the bottom and a bright field image at the top, which was not expected. In the least, we should expect the center light to provide bright field images at all heights. This analysis will continue in the 'Discussion' section.

5.2 Identification of Plasmodium Falciparum Parasite in RBCs

As previously mentioned, the amount of data is nearly endless since approximately 20 measurement rounds were made capturing images of the sample in all three geometries, in all thirteen spectral bands. Some images were captured with full resolution (2594x1944) meaning there are over 5 million spectra in one image. Due to the large amounts of memory required to even import a full resolution image into Matlab®, the resolution was often decreased. Most commonly, we used either 600 x 450 pixels or 1000 x 750. In one image there are generally 300-400 RBCs, depending on the concentration in that region. Due to the magnification of the system, one RBC contains roughly 200 pixels. Since primary analysis is aimed towards determining whether an RBC is infected or not, it is clear the amount of data available is nearly endless.

In this section we will present some true images in true color to get an overview of what a sample region looks like. Then some spectra will be shown of both infected and healthy individual RBCs. In addition, some contour maps of an RBC, displaying three-dimensional data will also be shown in an interactive way.

5.2.1 True Color Representation of a Sample

A true color image is displayed in such way that we humans would see it with our naked eye. 470 nm, 525 nm, and 625 nm were combined in matching ratios to match the function of the cones and rods on our retina. The spatial resolution of the three following images is 600 x 450 meaning there are 270 000 spectra available for analysis. The three following images are also taken over the exactly same spatial region so that each pixel contains spectral information from all three geometries (Fig. 5.2.1-1, 5.2.1-2, and 5.2.1-3)

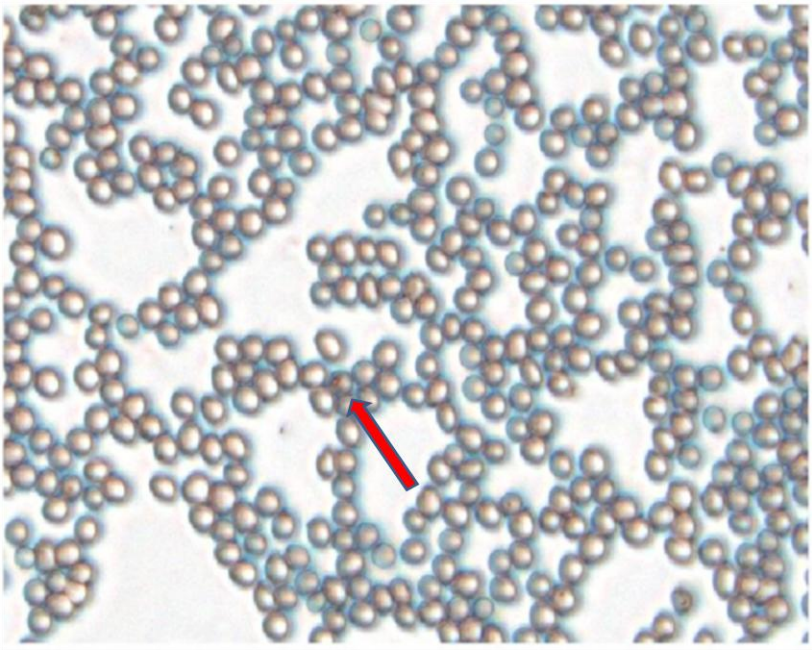

Fig. 5.2.1-1 This is a true color representation (combining wavelengths 470 nm, 525 nm, and 625 nm) of a blood sample with relatively low concentration of infected blood cells. There is only one clear infection which can be seen close to the center of the image where the red arrow indicates.

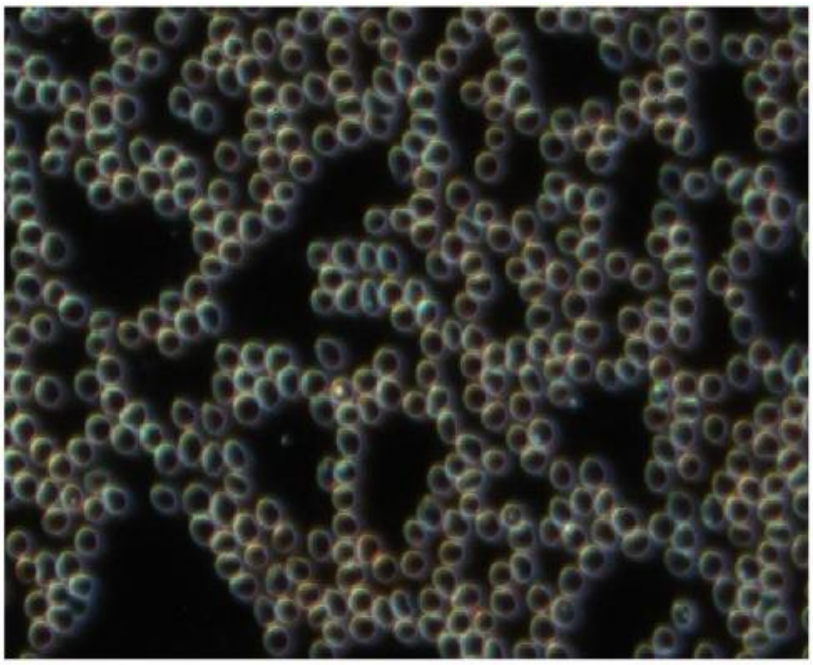

Fig. 5.2.1-2. This figure is clearly a dark field representation of the sample. In this image the parasite is quite clear in comparison to the transmission image. In this image potentially more parasites are visible; however, we must not forget that a true color image does not really give us any more information than our eyes can.

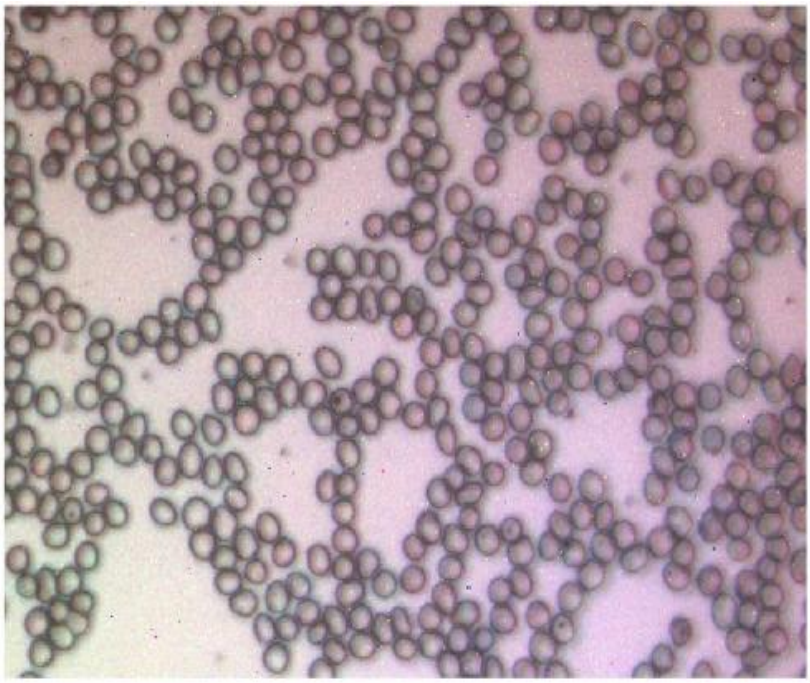

Fig. 5.2.1-3. This image is taken in reflection and deserves some discussion. In Fig. 5.2.1-1 it is expected that the background is bright since more light can pass through. Then, at first glance it makes little sense why a reflection image of the same sample also give a bright background. If light can easily pass through a sample from the bottom, we would expect that it would pass just as easily through the sample from the top, especially when the RBCs are equal in shape seen from both ends. This phenomenon can be well explained and is due to specular reflection of the glass slide, as was discussed in Sect. 1.1. Another thing to point out is that the illumination field is leaning diagonally down from the left down to the right. This could be for a few reasons such as components not being centered, the actual sample is leaning etc. However, most importantly it was accounted for as we created a virtual bright reference with a 3rd order polynomial plane which seemed to agree with the tilt seen.

Moving further with the analysis, the first close-up observation of an RBC will be to observe it in scattering mode (Fig. 5.2.1-2) since it seems at first glance to give the most contrast. Using a Matlab® script, created together with Mikkel Brydegaard, a protocol for mapping out individual RBCs was made. From these, spectra in all three acquisition modes were saved at all wavelengths. In addition, 3-dimensional

intensity contour plots were acquired for each RBC, both infected and healthy. For one cell, 3 spectra and 3 contour plots were saved.

5.2.2 Spectra of Infected and Healthy RBCs

The following results are taken over a specific region inside an RBC. The Matlab® script finds the center of the RBC (as well as it can be found) and from there marks out an area surrounding the center spot. This area can be extended simply by changing the value for the radius-cutoff in the program. It is quite hard to find an RBC with a perfectly round shape; we therefore chose the radius significantly shorter than the radius of the RBC to give the program a little wiggle-room to find the center. Across the diameter of one RBC there are approximately 25 pixels (counted for an RBC seeming to have an ideal shape). Knowing that from the center, the RBC will span approximately 12 pixels, we set the program to collect data within a radius of 6 pixels, which we found was enough to find good contrast in the spectra for many RBCs. The results are shown in Fig. 5.2.2-1

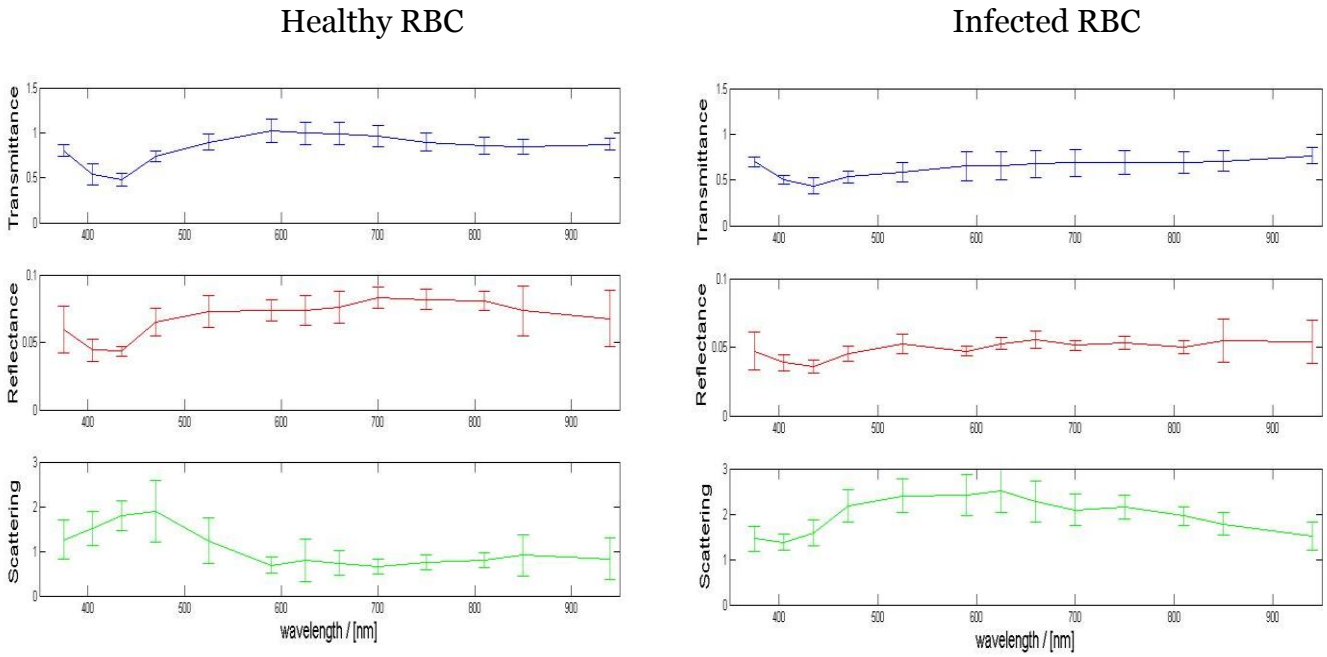

Fig. 5.2.2-1. On the left are the spectra for a healthy RBC in all three modes and on the right for an infected RBC. The scales are equally normalized in both sets of spectra.

Before we delve into the analysis of these spectra, we would like to point out that many spectra were generated and these results are well reproducible.

At first glance we can see that we are actually measuring on blood cells. The Soret Band previously discussed, is quite prominent in all spectra above. Since the instrument has not been previously calibrated, it is positive to see that it can characterize the general spectral shape of hemoglobin correctly. The next thing we notice is that there are some spectral regions which are quite different comparing the spectra for healthy and infected RBCs. The transmission spectrum for the infected RBC exhibits a general higher absorption in the region from 500-900nm. This could

be due to additional absorption from either the parasite itself or some waste product it creates from the hemoglobin it has consumed. This can also be seen in the reflectance data which makes sense since a photon will not be reflected if it has already been absorbed. The most interesting result lies in the scattering spectra. We can see that there is a broad scattering signal which seems to slightly peak at 625 nm. Comparing to the true color images in Fig. 5.2.1-2, we can see the broad white light shining in the center of the RBC, which compares nicely to the spectrum above. Although no extended statistical analysis will be covered here, it is worth creating a preliminary contrast function simply by observing the spectra since the observations suggest that acceptance criteria for malaria can be formulated based on the spectral features in Fig. 5.2.2-1.

5.2.3 Preliminary Contrast Function

Since there are three sets of spectra, we can create a three dimensional space in which we create a region defining malaria infection. Comparing the spectra for an infected and healthy RBC in each acquisition mode separately, we can find two wavelengths in each pair where the greatest contrast is created through division of these wavelengths (using two wavelengths is a good start, but there is no limitation in how many wavelengths can be used, as long as they seem to consistently create good contrast from sample to sample). In each mode, a wavelength-pair will be found which seems to exhibit the strongest contrast through division. That is, if I_{400}/ I_{700} yield a low number for a healthy RBC and a very high number for an infected RBC (I_{400} means the intensity at 400 nm and so forth), these are two wavelengths good for creating a strong contrast. We can then plot values from the two ratios along a line and perhaps say something like 'any value higher than X is malaria'. If there are two additional wavelengths, or as in our case an additional acquisition geometry, which seem to exhibit good contrast through similar procedure, these values can be plotted along an orthogonal axis where another threshold value is set and thereby creating a region where malaria is defined. Figs 5.2.3-1, 5.2.3-2, and 5.2.3-3 show the wavelengths chosen to create a space in 3-dimensions where malaria is defined.

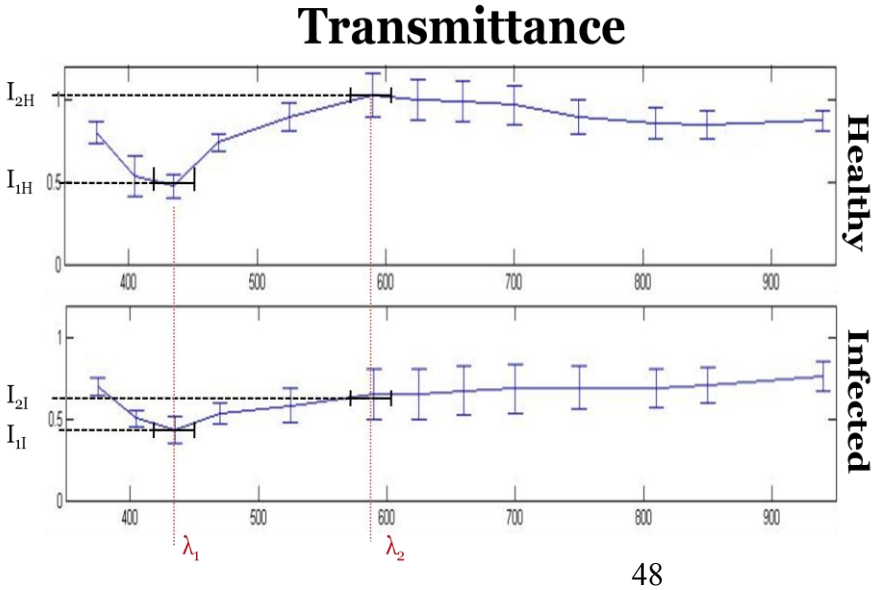

Fig. 5.2.3-1. The two wavelengths which seem to exhibit the strongest contrast in transmittance are λ_1= 435 nm and λ_2= 590 nm. The intensity values (as read from the graph) are I_{1H}= .5, I_{2H}= 1, I_{1I}= .48, and I_{2I}= .65. These wavelengths seem to give the strongest contrast although I_{1H}= I_1. The two ratios then become I_{2H}/I_{1H} = 2 and I_{2I}/I_{1I} = 1.35. The scale on the x-axis is [nm] and the y-axis is normalized intensity-

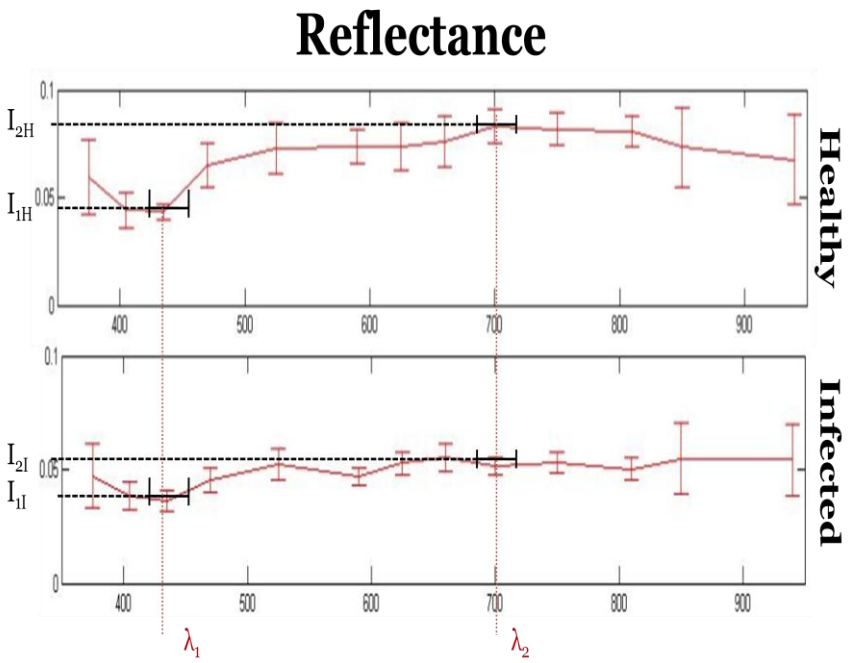

Fig. 5.2.3-2. The two wavelengths which seem to exhibit the strongest contrast in reflectance are λ_1= 435 nm and λ_2= 700 nm. The intensity values (as read from the graph) are I_{1H}= .45, I_{2H}= .85, I_{1I}= .38, and I_{2I}= .52. The two ratios then become I_{2H}/I_{1H} =1.88 and I_{2I}/I_{1I} =1.36.

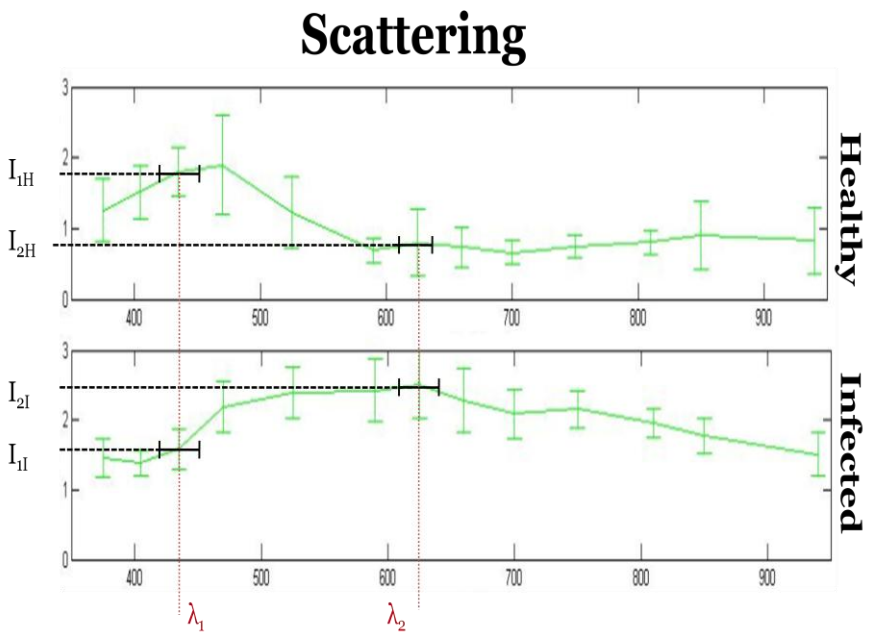

Fig. 5.2.3-3 The two wavelengths which seem to exhibit the strongest contrast in scattering are λ_1= 435 nm and λ_2= 625 nm. The intensity values (as read from the graph) are I_{1H}= .1.8, I_{2H}= .8, I_{1I}= 1.65, and I_{2I}= 2.5. The two ratios then become I_{2H}/I_{1H} =.44 and I_{2I}/I_{1I} =1.52.

Now we have our information to create the criteria for 'is malaria'. $T(I_{435}/I_{590})$, $R(I_{435}/I_{700})$, and $S(I_{435}/I_{625})$ can now be plotted in a 3-dimensional coordinate system and a threshold value for each 'variable' can be set. Remember that this is an example and a preliminary attempt to create some kind of contrast function and only one set of data is used. This process should be repeated for several RBCs so that error bars can be included which is important in order to set a threshold value which holds within the error of the measurement procedure or any other factors (i.e. different blood types, age of person, etc). Fig 5.2.3-5 shows how our contrast function creates a space in 3-dimensions. Any set of spectra that fulfil these criteria, we call malaria.

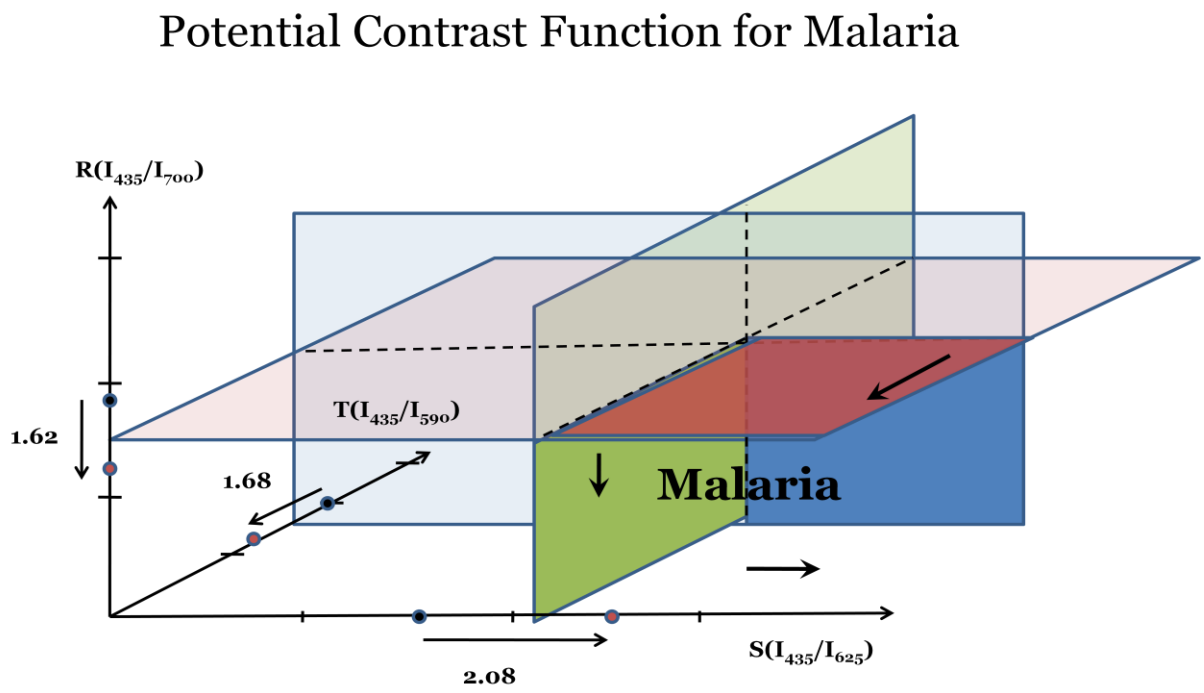

Fig. 5.2.3-5 The two intensity-ratios for each pair of spectra are plotted where the black dot represents the healthy RBC and red the infected one. The value shown in the image is the value exactly between the two intensity ratios. The Malaria region encompasses all values that fulfil the following criteria: $S(I_{435}/I_{625})>2.08$ and $R(I_{435}/I_{625})<1.62$ and $T(I_{435}/I_{625})< 1.68$. These criteria span out a block expanding in the direction indicated with the arrows and bordered by the planes. Using division of two variables means the values could never be a negative since that would mean the sample exhibits negative absorption or negative scattering. If this happens, it is a sign of the procedure not being carried out properly and reconsideration of references should be made.

From Fig. 5.2.3-5 we can understand that the more dimensions we add, the more sure we can be our results are correct. If we had only used reflectance and scattering data, malaria would have only been defined with an area without any information of depth. All points, for example $T(I_{435}/I_{590}) = 1$ as well as $T(I_{435}/I_{590}) = 5$, would all end up in the same area indicating an infection, but we know this is wrong from Fig. 5.2.3-5. To gain a higher signal-to-noise ratio, averaging over a certain spectral region can be performed. It should be noted that any forming of these ratios is a pictorial and pedagogical representation of what a more complete multivariate analysis can achieve.

5.2.4 Contour Maps with Radial Dependence

The next set of data is represented in what is a called 3-dimensional contour map. Since a normal RBC is homogenous without any specific structure, we were interested in finding the spectral characteristics as a function of radius. Ideally, the RBC should be perfectly round, which of course is not the case, but it is interesting to see if the differences between a healthy and infected RBC has any radial dependence. The three sets of contour maps are produced with the same data as for the spectra in Fig. 5.2.2-1. The three dimensions presented in the contour maps below are radial distance (x-axis), wavelength (y-axis) and intensity (z-axis scale) Fig. 5.2.4-2, 5.2.4-3, and 5.2.4-4. The radius was determined by putting a known width reference in the field of view and measuring how many pixels it spanned. One important thing to

keep in mind when looking at the contour maps is that the spectra generated above in Fig. 5.2.2-1 were limited to a radius of 1.5 μm where the color maps represent data from 3 μm. This can be seen in Fig. 5.2.4-1 where the two RBCs from which the data was collected are shown (scattering).

Healthy RBC (true color) Infected RBC (true color)

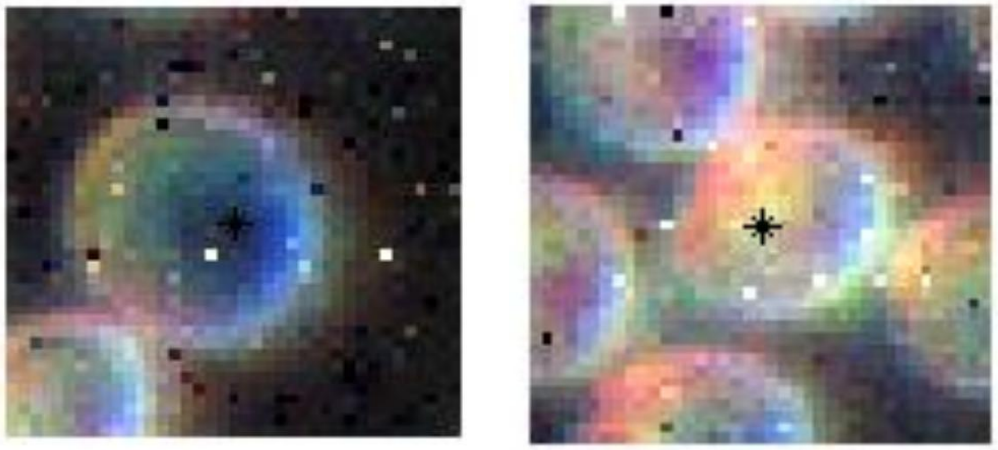

Fig. 5.2.4-1. These are the two RBCs from which both the spectra above and the contour maps below have been generated. They are displayed in a true color, dark field image. The RBCs are from one and the same blood sample and we can clearly see a difference. We can also see that the program didn't perfectly find the middle of the RBC which is why we gave it some margins. But even within these margins, we should be able to detect a difference between a healthy and infected RBC.

Healthy RBC (transmittance) Infected RBC (transmittance)

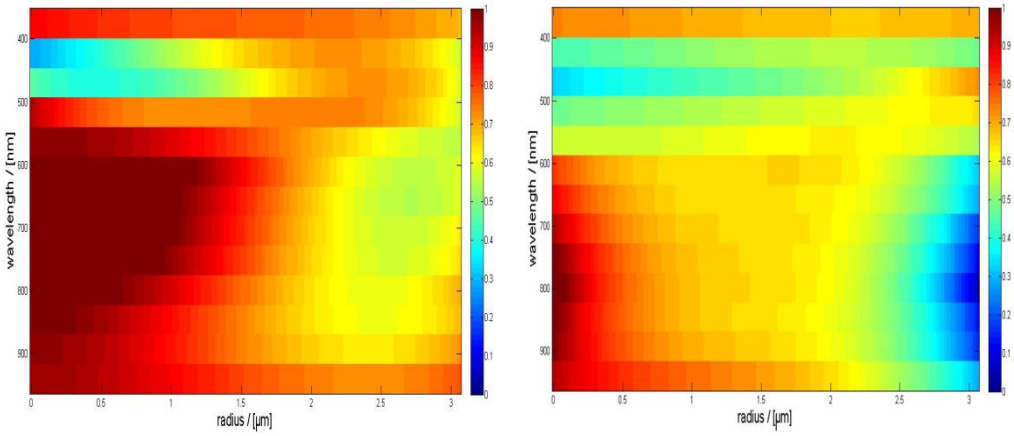

Fig. 5.2.4-2. First we can see that these contour maps agree well with the spectra in Fig. 5.2.2-1 up to the radial distance set as the threshold above Comparing these contour maps to the true color images above we see the similarities.

Healthy RBC (reflectance) Infected RBC (reflectance)

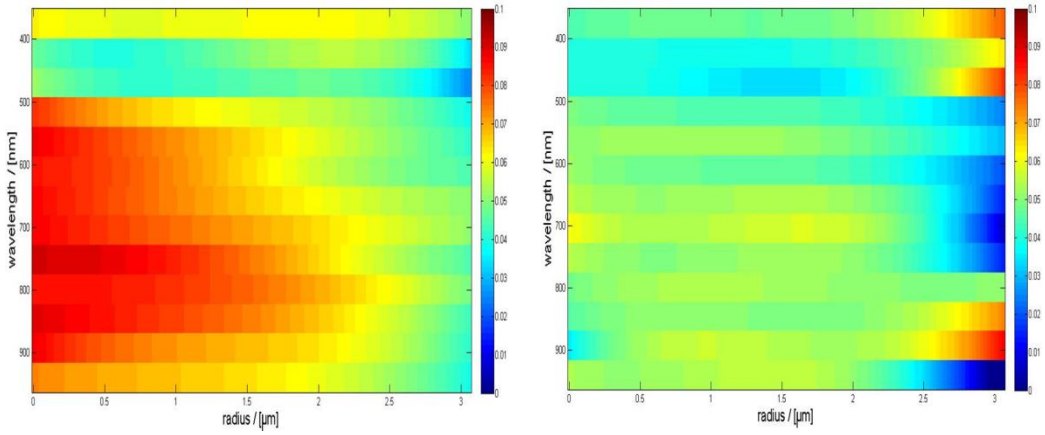

Fig. 5.2.4-3. The reduced reflectance is clearly seen in the infected RBC. There seems to be a slight increased reflectance towards the edge which could have something to do with the shape of the RBC along with the angle at which the light impinges [12].

Healthy RBC (scattering) Infected RBC (scattering)

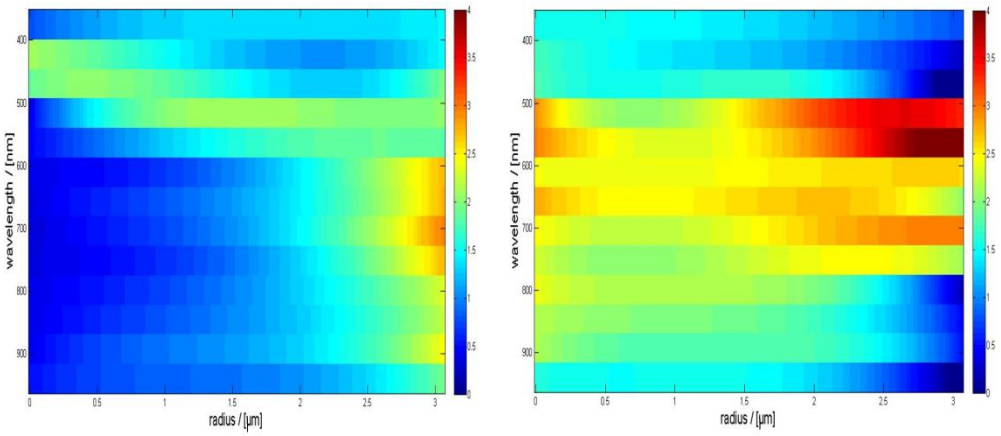

Fig. 5.2.4-4. Here we can clearly see a structure in the infected RBC that seems to fill the entire region of interest. This mode was previously expected to give good contrast, which we now can see. Again, the shape of the spectra agree well with that of Fig. 5.2.3-2

The contour maps provide an interactive way to represent data and are useful to draw general conclusions; however, to create a contrast function or to do any kind of multivariate analysis, it is easier to observe the 2-dimensional spectra. A final image will be shown of a heavily infected sample where the spectral characteristics observed above can be well seen. (Fig. 5.2.4-4)

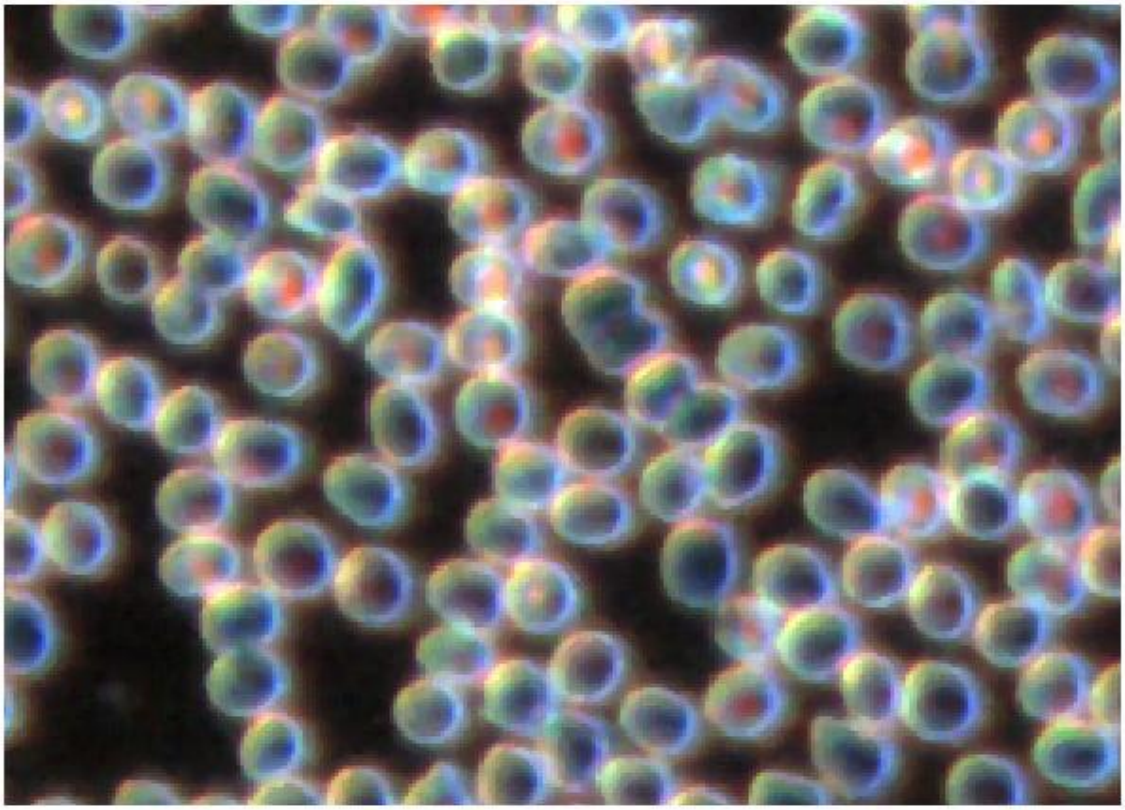

Fig. 5.2.4-4. This image is taken in scattering mode. Due to the strong scattering from the high concentration of RBCs, the signal was very strong and reduced by a factor 4 over the entire image. A median filter has been applied to remove the 'salt & pepper', where pixels were combined in 3x3 bins and the median intensity value of the 9 pixels was chosen and applied to all. The image therefore appears a little blurry, but since there are a lot of pixels on the imaging-chip of the camera, we have the freedom to apply these functions and still have a good resolution. Remembering two things: healthy RBCs do not have an internal structure, and that healthy RBCs exhibit strong scattering towards blue and infected towards red, we can draw solid preliminary conclusion by simply viewing this image in true color. However, a more definite conclusion will be drawn after statistical methods have been applied.

5.3 System Spectral Bands

Clearly, it is very important to know exactly how the LEDs emit. An Ocean Optics USB4000 spectrometer was used to characterize the bands in each geometry. All geometries are plotted on the same graph to also see how well they align. It is good to know that e.g. 810 nm in reflection also is 810 nm in transmission or scattering (See Fig. 5.3-1)

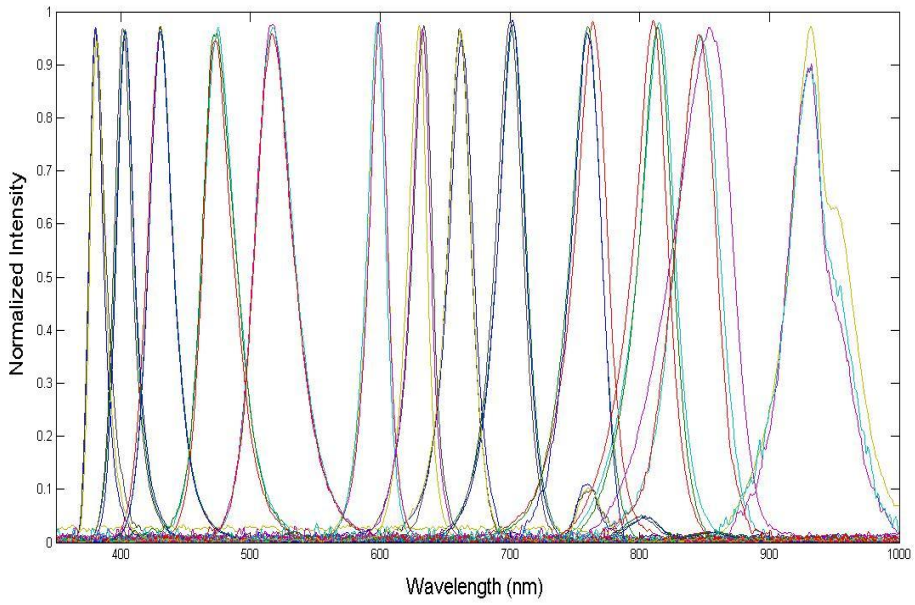

Fig. 5.3-1. The emission bands in all three geometries seem to overlap quite well. The peak emission for each LED agree well with the values used while building the spectra above. At 780 and 800 we can see small peaks and these are due to the spectrometer measuring 2nd order harmonics of the first two bands (375 nm and 400 nm). We can see that the spectral bands between geometries are slightly shifted in the IR. This could be because the bandgap voltage for IR LEDs is much smaller which makes them more susceptible to temperature variances.

Discussion

The discussion section is meant to cover any further reasoning left out from a previous section as well as pull together all the main points made throughout the paper and provide a final resolution to the thesis. In the previous section much discussion was provided since it made more sense to bring up some points in the immediate context for better clarity.

6.1 Difficulties during Design Phase

During the period in which the instrument was designed and put together there were a few issues that were encountered. Some were more technical and only needed time and effort to solve, and some were more basic where a decision needed to be made of how the design should proceed.

One issue that consumed copious amount of time to resolve, which does not really need its own paragraph to discuss, was the electronics. Several weeks were spent on trying to get the controller to work the way we intended it to work. The main problem that insisted in showing up was the switching of LEDs and how they refused to switch on one by one. All the electronics will be presented in Appendix I, but for now it is worth mentioning that almost all problems were solved using *bipolar junction* transistors (BJTs) instead of *field effect* transistors (FETs).

6.1.1 Overcoming Chromatic Aberration

At this point the reader is well aware of the purpose for using most of the components and how they intended to direct light. Much time was allocated towards deciding how to implement the different modes using components which had little or no effects due to chromatic aberration. The reflective objective has been covered significantly and any further discussion around this is not necessary. Although one thing to add is that we did not consider all components with regard to minimizing chromatic aberration, but the objective is the main component since it is in this component the signal from the sample will undergo the most magnification. That means that through the objective light will undergo heavy reshaping which would in a dispersive objective mean that the wavelengths would be separated more here than anywhere else in the instrument. A quartz lens was used for reasons already discussed in Sect. 1.6.2, but there are other lenses in the microscope which also could have been replaced with this type of lens. These options were not explored since these lenses were well integrated in the original microscope and we figured it would be better to put the system together using these original components to see how it worked. Apparently, good images were in general produced so no further effort was put towards exchanging these. However, after some time we noticed that there were some issues when we tried to observe the fluorescence from chlorophyll on leaves. Very weak signals were measured and we were not sure if it was the illumination or the sample emission. We realized that most of these lenses were coated and suspected this could have something to do with the reduced UV signal. On a leap of faith we decided to remove some of these lenses (some with a little bit of brute force) and the observed fluorescence increased. It was then realized that most of these lenses were coated to optimally transmit visible light, which thereby caused problems when we tried to illuminate with UV.

Another component we discussed previously which seemed to cause some issues was the polka-dot beam splitter (PDBS). During design, the reason for using it was to achieve an even transmittance for all wavelengths. A normal beam splitter does not exhibit chromatic aberration in the same sense we have been discussing, but rather it chooses to transmit some wavelengths more than others. Unlike the PDBS, beam splitters are generally optimized for relatively short wavelength region. However, once integrated in the system, the polka-dot beam splitter started showing some odd behaviour. In some images we noticed there was some systematic blurring. We finally realized that the polka-dot beam splitter was acting as a transmission

grating creating higher order diffractions in the image due to its periodic structure of holes and mirrors. This was quite undesired so we removed it and replaced it with the original beam splitter.

6.1.2 Bright Field or Dark Field?

This issue has already been extensively discussed in the previous section as we saw that the fiber ring light (FRL) can be used for creating both. However, our reasoning with regard to the light emerging from the center did not seem to agree well with what we saw. Further testing was made and it seems there is a position where the light intensity measured at the detector reaches a peak value. But there are some things to consider with this. The light intensity incident on the lens will vary significantly depending on the height of the assembly. The opal diffuser provides a Lambertian distribution and the intensity falls off according to the 'inverse-squared law', meaning the intensity is proportional to the radial distance from the source squared. Also, as the assembly is raised, the acceptance cone for the lens decreases. It is therefore hard to theoretically predict the behaviour of the 'center light' as a function of height and this will be left to be determined through more controlled experiments beyond the scope of this project.

6.2 Final Conclusion

The work entailed by this project was an extension to a previous LED microscope purchased and built for $200. The first version was applied to measuring *plasmodium* malaria. The purpose was to extend the capability of that microscope and invest an amount of money justified by its capability and applicability. The total cost of the upgraded microscope was roughly €5000, which is a very cheap scientific instrument, especially when its applicability is of great relevance to the Third-World.

The research and analysis performed on the malaria parasite has yielded very interesting preliminary results. We were able to create bright field, dark field as well as reflectance images of both an infected and healthy red blood cell. The spectra obtained from these blood cells agree very well with accepted data. Extensive analysis was not performed, but this will be done in the near future to extend the research to properly identify the various stages of malaria.

Also working in collaboration with all the groups from Cote D'Ivoire, Ghana, Senegal, Kenya, Mali, and Sri Lanka has sparked much motivation to conduct this type of research and explore new applications has grown. It is of great importance for science in the Third-World that they can conduct their own research and actively apply this knowledge to problems of regional interest.

Malaria has been spectrally identified and contrast has been seen between a healthy and infected blood cell using an LED multispectral microscope in all three illumination modes. The stepping stone for future research has been set upon which efforts will be made to build a solid foundation in this type of research.

Acknowledgements

The work presented in this thesis could not have been possible without the help and dedication from many people and organizations. The financing from the International Science Programme (ISP) and hospitality of the Laser & Fibre Optics Center (LAFOC) has been of central importance. Without the following people I would not have had the knowledge or the confidence to perform this work:

With an experience of a lifetime and seemingly endless energy, my supervisor Sune Svanberg has been of tremendous support providing advice, ideas, and understanding in the field of *Applied Spectroscopy*. He is a rich source of inspiration and I highly value his optimism and dedication.

I thank Mikkel Brydegaard for sharing his intelligence and profound knowledge within several scientific fields. He is a great teacher and working closely with him has undoubtedly provided a deeper understanding of optics and imaging amongst many areas.

I am especially thankful for Jeremie Zoueu and his family for making my stay in Côte D'Ivoire an utmost pleasant experience. I admire his devotion to malaria research and acknowledge that this project would not be a success without his initiative.

Many thanks goes to the members of the *Applied Spectroscopy and Remote Sensing* group for their utter willingness to answer any questions or provide help in any way. I am impressed with their hard work and am confident in their future success.

Working within the Atomic Physics Division has been a pure pleasure and I thank all members for showing me respect and good friendship. I believe this atmosphere lays a good foundation for great research.

My family has been a true blessing and I thank them for their love and support. They have helped me in every way possible and for that I am grateful.

Last, yet not in the least, I give all my thanks to God for surrounding me with good and intelligent people and providing me with this opportunity. He has truly blessed my life and any credit received, I give to Him.

Appendix I: *Electronics*

The electronics provides three constant current sources as well as a way for controlling the LED switching. Since there was much interest in creating an automated system, the electronics had to be designed accordingly. To Fig. I-1 is a simplified layout of how an LED is connected and switched on-off. Unless the multiplexer switches an LED on, there is no current flowing from the top down to ground and no light is emitted.

The three boxes indicate the three separate circuit boards which are inter-connected through flat-cables. Further explanation of how each section works will be given below.

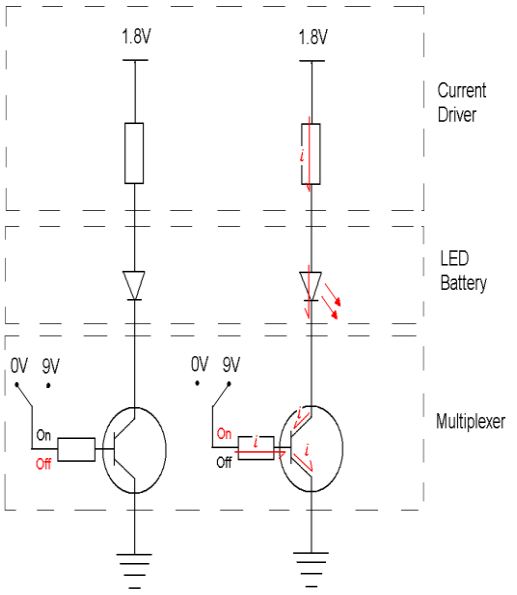

Fig I-6. An overview of how the LED switches on and off. For an LED to light current must have an open path to flow from the top down through the LED to ground.

I.1 Current Driver

Fig I.1-1 is a schematic overview of the constant current driver. For this microscope, three current sources are needed so the schematic below is repeated three times creating the output values indicated by I_1, I_2, and I_3.

The circuit works in such way that the three diodes (1B4148) limits the voltage at the positive input of the operational amplifier (LM324) to approximately 1.8V (3x 0.6V).

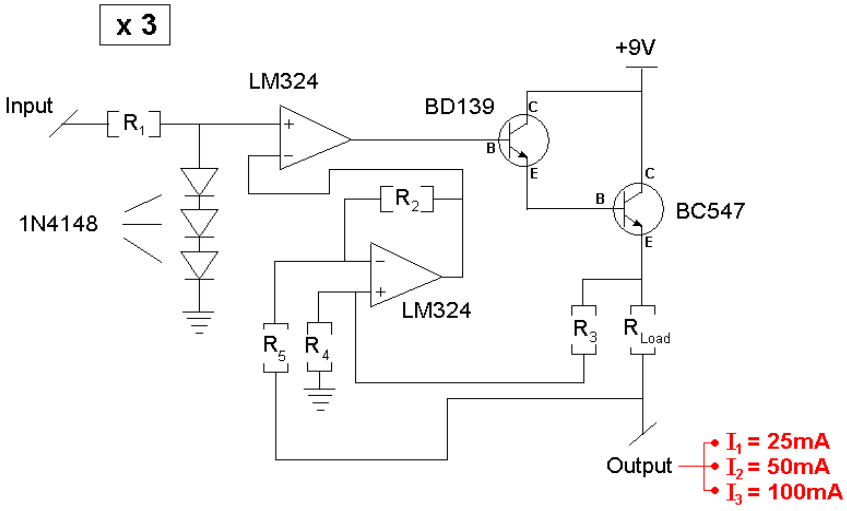

Fig. I.1-1 shows the constant current driver. Resistors R_1 – R_5 have 10 kΩ resistance. R_{Load} regulates the current at the output according to Ohm's Law. The input comes from the analogue output from the DAQ where the signal has been amplified from 5 V to 9 V before reaching the current driver circuit. The three diodes (1N4148) are limiting the voltage at the positive input of the first Op-Amp to roughly .6x3=1.8 V.

The output of the op-amp (operational amplifier) is initially 1.8V, which is acquired by subtracting the negative input (initially zero) from the positive. The two bipolar junction transistors (BD139 and BC547) are used to provide an amplified current path from the operational amplifier to the load resistor. They are both of npn structure which means that the current is generated by the movement of excess electrons rather than holes. Any current at the base is amplified at the collector and the amplification depends on how the semiconductor materials have been doped.

The circuit in Fig. I.1-1 is designed so that it provides what is called 'negative feedback', which is common when stabilizing amplification circuitry. If at any point the amplification is too large, the circuit corrects this by subtracting the excess amplification from the original signal causing the next round to be corrected with the same amount. It works similarly in reverse where insufficient amplification will increase the initial signal.

The voltage at the front end of the load resistor is approximately 1.8V (initially set by the three diodes) since the impedance across the base and emitter on the two BJTs is negligible when they are switched on (if the transistors are forward biased). In order to switch on an LED, the path from the current driver output down to ground should be connected so that current may flow through the LED and for emission. This is controlled with the multiplexer.

I.2 Multiplexer

The multiplexing circuit consists of a 4 bit, 16 channel decoder converting a 4-bit input to 16 unique addresses. The microscope only utilizes thirteen LEDs, hence only outputs 0-12 need to be connected. Each output has a unique binary address which is accessed by a data acquisition card (DAQ), which in turn is controlled by the computer. The DAQ interfaces the computer with the electronics and is discussed separately.

As an address on the decoder is called by the DAQ, the output goes from 0V to 9V and thereby connects the path from the current driver, through the LED, to ground as illustrated in Fig. I.2-1. Since each output is uniquely addressed, only one LED can be lit at a time. However, from the emitter of the transistor connected to the decoder, there are three similar LEDs connected, each belonging to a separate LED battery. Therefore, as one output of the decoder goes high, three LEDs are lit. However, unless current is provided to the LED as well, it will not emit light. Therefore, the multiplexer and the current driver work in conjunction to only light one LED at a time.

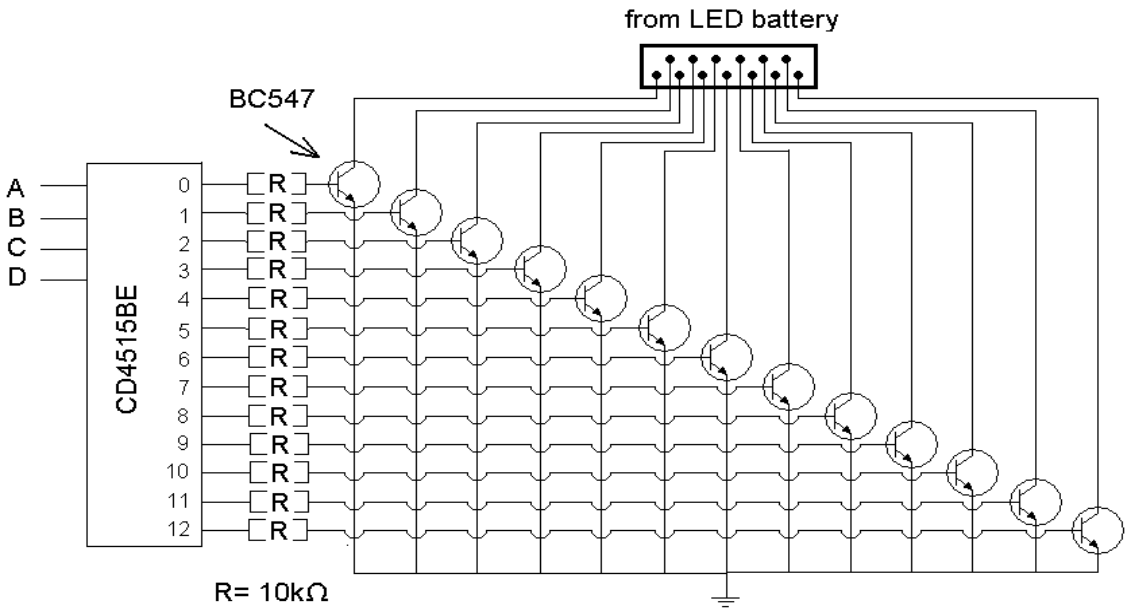

Fig. I.2-1. A schematic overview of how the multiplexer 'allows' a path to ground to which current may flow from the LED and thereby lighting it. No LED will be lit if either the current driver is not providing any current or if the multiplexer is not opening the path to

I.3 LED Battery

The LED battery is bridged between the multiplexer and the current driver. It is connected through a flat-cable. A schematic of how the LEDs are connected is shown in Fig. I.3-1. One or more LEDs share an anode as 13 LED chips in 9 physical housings are arranged so that their central axis of illumination strikes the same point (as discussed in Sect. 4.1.1).

The LED battery is connected between the multiplexer and the constant current driver on a separate board. No switching is done here and light will be emitted if current is allowed to flow from the current driver through the multiplexer to ground. Fig. I.3-1 shows the 13 LEDs and their peak emission wavelengths.

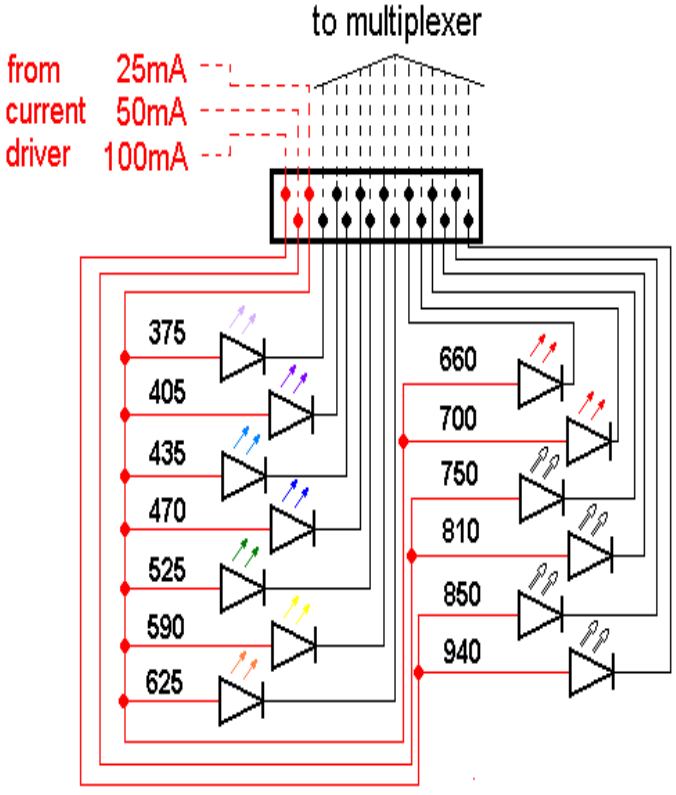

Figure I.3-1. A schematic of the LED battery. Three of these provide lighting for scattering, transmittance, and reflectance measurements.

I.4 Data Acquisition Device (DAQ)

The DAQ bridges the computer and the electronic circuitry so that data can either be measured or controlled through software. The DAQ has the ability to output both analogue and digital signals between 0-5 V in several channels. It also has the ability to measure an analogue signal. Fig. I.4-1 shows the port schematic of the DAQ (Model USB-6009 from National Instruments).

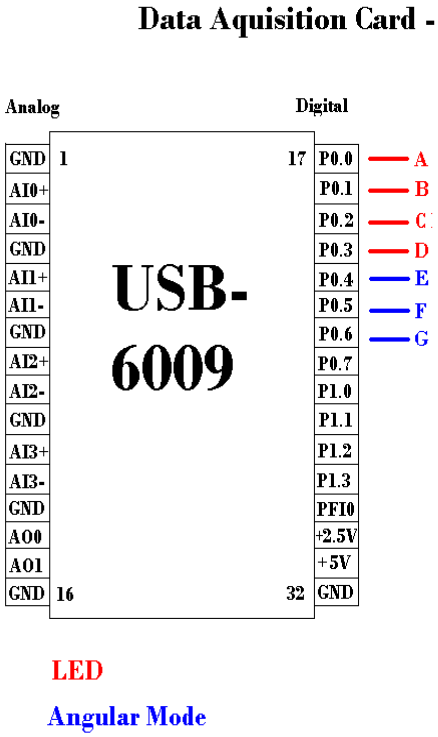

Inp. D	C	B	A	Outp.
0	0	0	0	0
0	0	0	1	1
0	0	1	0	2
0	0	1	1	3
0	1	0	0	4
0	1	0	1	5
0	1	1	0	6
0	1	1	1	7
1	0	0	0	8
1	0	0	1	9
1	0	1	0	10
1	0	1	1	11
1	1	0	0	12
1	1	0	1	13
1	1	1	0	14
1	1	1	1	15

G	F	E
0	0	1
0	1	0
1	0	0

Fig. I.4-1. On the left the analogue I/O, and on the right the digital I/O are represented. The truth table to the right shows how a combination of digital outputs creates a unique address. The red lines indicate the ports controlling the LEDs and since only 13 LEDs are used, the last three channels are not used for LED switching, but rather for current controlling (as mentioned above). The current controller ports are indicated with blue and will only switch on one at a time unless illumination is desired in more than one geometry simultaneously. It should be mentioned that the created software only allows for one of these 'blue' lines to be high at a time.

Appendix II: *Measurement Procedure*

One of the main reasons for creating this microscope was to be able to extract spectra for scattering, transmittance, and reflectance from the same spatially discretized region. Since the pixels are so small physically, and appear even smaller with the system magnification, it is important that the sample does not move between each acquisition sequence.

Each acquisition mode required three rounds of measurements (sample, bright and dark references) so careful consideration was required when performing a complete measurement set. A total of 9 measurement rounds were made and how they were performed, as well as in which order, is presented in Fig. II-1

	Reflection	Scattering	Transmission
Bright Reference	**[5]** Opal diffuser with white surface facing up.	**[6]** Opal diffuser with white surface down.	[1] Empty part of the slide with minimal dirt
Dark Reference	**[7]** Nothing	**[8]** Nothing	**[9]** Power unplugged
Sample	[2] Normal	[3] Normal	**[4]** Normal

II-1. Each square represents a measurement set taken for all wavelengths. There was however only three acquisition protocols set for each geometry which then were applied to the other two measurements. The order in which the measurements were made is indicated by the number. The red numbers indicate the rounds where the acquisition protocols were set.

The table in Fig. II-1 presents a specific order for the measurements made on the malaria parasite. One important thing to consider is whether the sample or the bright reference gives the strongest signal because this should decide which is used to set the acquisition times in the protocol. Problems can arise if, for example the protocol-times for a mode is set according to Fig. II-1 and when the bright reference for that mode is taken, the image reach saturation in many bands. The acquisition times would then have to be reset and the entire procedure would have to restart, which can be frustrating if a good region of the sample had been found. It is therefore advisable to check whether the sample or the bright reference gives a stronger signal and use the strongest to set the acquisition protocol.

Appendix III: *LabView™ Acquisition Program*

The DAQ controls the electronics as told by the computer. Either LabView™ or MatLab™ can be used to control it. We chose to use LabView™ since it could control the camera much better. This section will briefly describe how the program works and how the microscope is controlled. There will be a number of screen-shots with the necessary information described on the side.

LabView™ has what is called a *front panel* (FP) where the program interfaces with the user and a *block diagram*, where the actual programming is made and executed. It is in the FP the user can set the different LEDs or geometry desired. The exposure time and gain of the camera can also be set and a live update of the object is constantly shown. See Fig. III.1-1

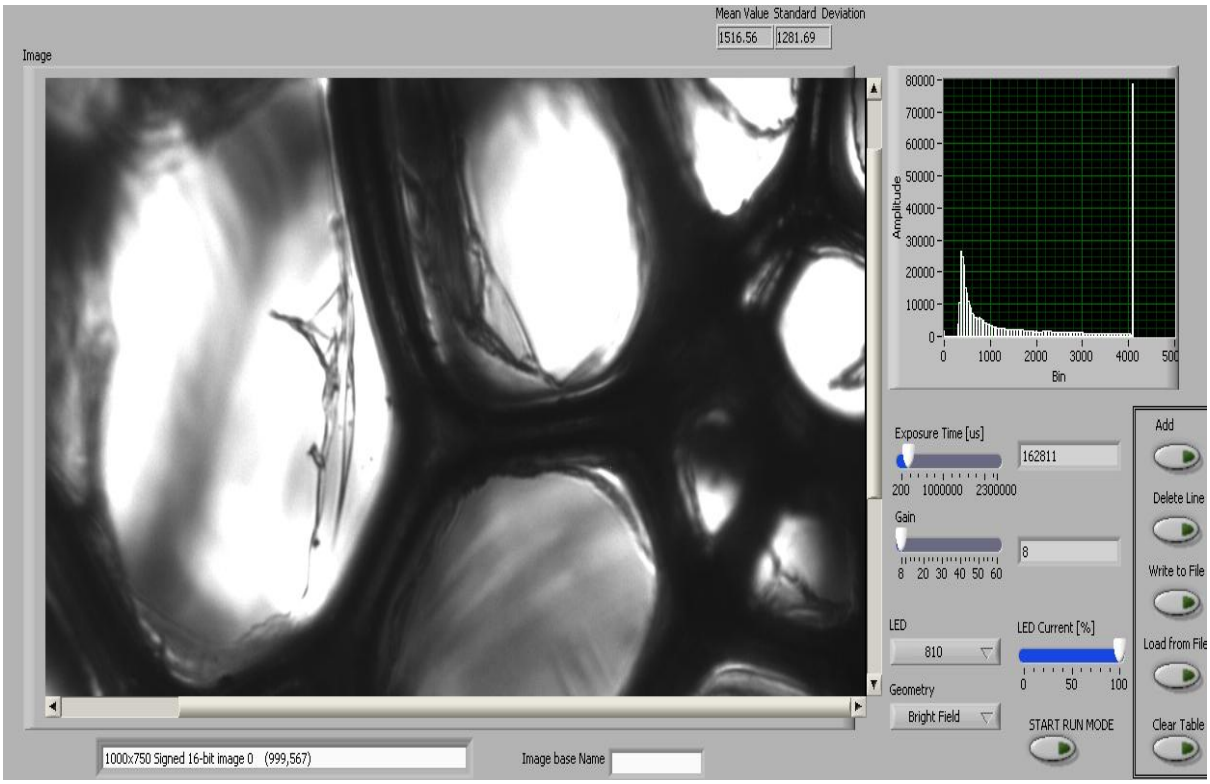

Fig. III.1-1. The object is a piece of foam viewed with a plan objective with 4x magnification. As seen on the right, the user can control the LED Current (from 0-100%) which comes in hand when wanting to take background images. The LED and the geometry can also be chosen, as well as the exposure time and gain.

In the upper right corner we see a histogram which counts the number of pixels that fall into each intensity bin. Since the camera is has a bit-depth of 12, it can distinguish between 4096 intensity levels. The last bin has by far the most counts which is a representation of the image being saturated. We can see that there are lot of very bright areas. It would be highly improbable that all these bright pixels represent an intensity falling exactly into the 4095^{th} bin, so we can draw the conclusion that the image is saturated in some regions and either the exposure time, gain, or the LED current should be reduced.

On the bottom left is some information of the capture settings for the camera such as image size, pixel depth etc. To the right is a field called 'Image Base Name'

and it's important that every time a measurement round is made, the experimenter should remember to put a name for future reference so that data is neither replaced, nor forgotten about.

In this mode the user can change the aforementioned settings while receiving a live update with a minimal delay (it was noticed that this delay is quite longer whenever a higher gain is used which will create bad images during an automatic capture). Once the user is satisfied, clicking the 'Add Line' button will enter the settings into a spreadsheet where they can be accessed at a later point. Then the user can add another LED with new settings and so forth. Once satisfied, the automatic protocol can be saved as an .xls file (Write to File), or the protocol can be directly executed (Start Run Mode). Once executed, the protocol will go to the specific .xls file and look up the settings line for line, apply them to source and detector and capture a picture. (Fig. III.1-2).

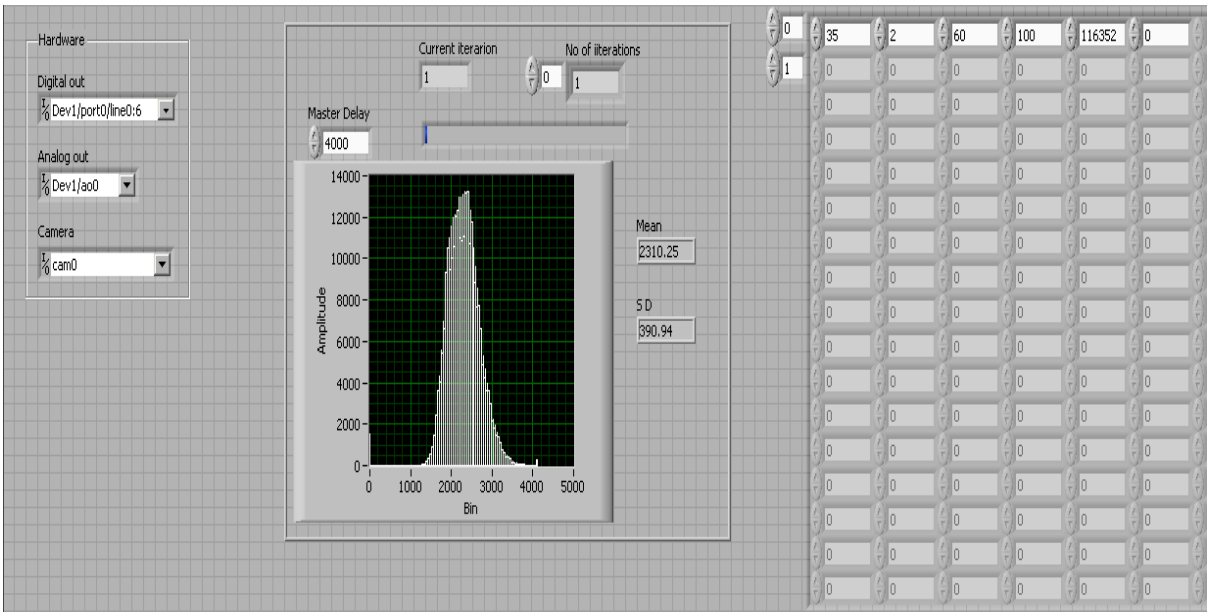

Fig. III.1-2. During the auto run mode the histogram for each image taken can be seen to assure that a good picture was taken. The master delay between each capture can also be set (in ms) if there seems to be a lag in response from the camera between captures. This is indicated by some of the images being completely saturated followed by some being almost completely dark. On the right are also the camera and DAQ settings. If the program complains about the DAQ or the camera not being present, check these settings to make sure they represent the proper ports etc.

The program can either operate in live mode where the image is seen and changes apply as you make them, or you can run in automatic mode where pictures are captured and saved according to an already set protocol.

Fig. III.1-1 and Fig. III.1-2 show the user interface and how to control the microscope. The block diagram is quite intricate and would be best understood if viewed in LabView™ where cursors explain what the software components do. Therefore these will be left out at this point.

References

[1]. Haitz Law – Nature Photonics 1, 23 (2006)doi:10.1038/nphoton.2006.78

[2]. X. Wu, J. Thigpen, S.K. Shah: *Multispectral Microscopy and Cell Segmentation for Analysis of Thyroid Fine Needle Aspiration Cytology Smears,* 31st Annual International Conference of IEEE EMBS, Minneapolis, Minnesota, September 2009.

[3]. S. Fatini, M.A. Franceschini, J.B. Fishkin, B. Barbieri, E. Gratton: *Quantitative determination of the absorption spectra of chromophores in strongly scattering media: a light-emitting-diode based technique*, Applied Optics, Vol. 33, No.-22, August 1994.

[4]. M. Brydegaard, Z. Guan, S. Svanberg: *Multispectral Broad-band multispectral microscope for imaging transmission spectroscopy employing an array of light-emitting diodes*, Am. J. Phys., Vol 77, No. 2, February 2009

[5]. B.E.A Saleh, M.C. Teich: Fundamentals of Photonics, 2nd edition, John Wiley & Sons (2007),

[6]. H. A. Haus: *Waves And Fields in Optoelectronics, Prentice Hall Inc. (1984), p31*

[7]. C. F. Bohren, D. R. Huffman: *Absorption and Scattering of Light by Small Particles,* John Wiley & Sons (1983), p 22,27-28.

[8]. P. Grosse and V. Offermann: *Analysis of Reflectance Data Using the Kramers-Kronig Relations*, Appl. Phys. A 52, 138-144 (1991)

[9]. S. Svanberg: *Atomic and molecular spectroscopy, 2nd edition*, Springer-Verlag, p. 66, (1992)

[10]. M. A. Paesler, P. J. Moyer: *Near-Field Optics: Theory, Instrumentation, and Applications,* John Wiley & Sons, 1996, p 5

[11]. M. Hammer, D. Schweitzer, B. Michel, E. Thamm, A. Kolb: *Single scattering by red blood cells,* Applied Optics, Vol 37, No. 31, November 1998.

[12]. A. M. K. Nilsson, P. Alsholm, A, Karlsson, S. Andersson-Engels: *T-matrix computations of light scattering by red blood cells,* Applied Optics, Vol 37, no 19, May 1999.

[13]. D. H. Tycko, M. H. Metz, E. A. Epstein, A. Grinbaum: *Flow-cymetric light scattering measurements of red blood cell volume and hemoglobin concentratoin,* Applied Optics, Vol.24, No. 9, May 1985.

[14]. M. Shahrooz Amin, Y. Park, N. Lue, R. R. Dasari, K. Badizadegan, M. S. Fiueld, G. Popescu: *Microrheology of red blood cell membranes using dynamic scattering microscopy,* Optics Express, Vol.15 No. 25, December 2007

[15]. B. A. Scalettar, J.R. Swedlow, J.W. Sedat, D.A. Agard: *Dispersion, aberration and deconvolution in multi-wavelength fluorescence images*, The Royal Microscopical Society, (1996)

[16]. S. Shah: *Segmenting Biological Particles in Multispectral Microscopy Images*, IEEE Workshops on Applications of Computer Vision (WACV'07), 2007

[17]. S. Svanberg: *Multi-Spectral Imaging, (2008)*

[18]. T. King: *Human Colour Perception, Cognition and Culture. "Why 'Red' is always Red,* The Society for Imaging Science & Technology Reporter 'The Window of Imaging', Vol. 20, No.1, 2005, p. 2

[19]. R. W. Cole, J. N. Turner: *Light-Emitting Diodes Are Better Illumination Sources for Biological Microscopy than Conventional Sources,* Microsc. Microanal. 14, 243–250, 2008

[20]. Y. Park, T. Yamauchi, W. Choi, R. R. Dasari, M. S. Field: *Spectroscopic phase microscopy for quantifying haemoglobin concentrations in intact red blood cells,* Optics Letters, Vol. 34, No. 23, December 2009

[21]. V. V. Tuchin, R. K. Wang, E. E. Galanzha, D, M. Zhestkov: *Scattering model of whole blood at haemoglobin glycation monitored by refractive index measurements with OCT, 2004 Optical Society of America, OCIS codes: 170.4500, 170.1470*

[22]. T. K. Mutabingwa, D. Anthony, A. Heller, R. Hallett, J. Ahmed, C. Drakeley, B. M. Greenwood, C.J.M Whitty: *Amodiaquine alone, amodiaquine+sulfadoxine-pyrimethamine, amodiaquine+ artesunate, and artemether-lumefantrine for outpatient treatment of malaria in Tanzanian children: a four-arm randmoized effectiveness trial*, The Lancet, Vol 365, April 23, 2005, p. 1475

[23]. M. Toda: *Life Cycle of Malaria,* U.S. Centers for Disease Control and Prevention, Oct, 2009, (abstract)

[24]. M. Brydegaard, A. Merdasa, S. Svanberg: *Multimode imaging spectrometer for angular resolved optical diagnosis on microscale*, to appear.